Manuscript submitted to **Biophysical***Journal*
Article

Spontaneous curvature, differential stress, and bending modulus of asymmetric lipid membranes

Amirali Hossein[1] and Markus Deserno[1,*]

[1]Department of Physics, Carnegie Mellon University, Pittsburgh, PA 15213, USA
[*]Correspondence: deserno@andrew.cmu.edu

ABSTRACT Lipid bilayers can exhibit asymmetric states in which the physical characteristics of one leaflet differ from those of the other. This most visibly manifests in a different lipid composition, but it can also involve opposing lateral stresses in each leaflet that combine to an overall vanishing membrane tension. Here we use theoretical modeling and coarse-grained simulation to explore the interplay between a compositional asymmetry and a nonvanishing differential stress. Minimizing the total elastic energy leads to a preferred spontaneous curvature that balances torques due to both bending moments and differential stress, with sometimes unexpected consequences. For instance, asymmetric flat bilayers, whose specific areas in each leaflet are matched to those of corresponding tensionless symmetric flat membranes, still exhibit a residual differential stress, because the conditions of vanishing area strain and vanishing bending moment differ. We also measure the curvature rigidity of asymmetric bilayers and find that a sufficiently strong differential stress, but not compositional asymmetry alone, can increase the bending modulus. The likely cause is a stiffening of the compressed leaflet, which appears to be related to its gel transition, but not identical with it. We finally show that the impact of cholesterol on differential stress depends on the relative strength of elastic and thermodynamic driving forces: if cholesterol solvates equally well in both leaflets, it will redistribute to cancel both leaflet tensions almost completely; but if its partitioning free energy prefers one leaflet over the other, the resulting distribution bias may even create differential stress. Since cells keep most of their lipid bilayers in an asymmetric nonequilibrium steady state, our findings suggests that biomembranes are elastically more complex than previously thought: besides a spontaneous curvature they might also exhibit significant differential stress, which could strongly affect their curvature energetics.

STATEMENT OF SIGNIFICANCE The two leaflets of biological membranes generally differ in their lipid composition, but we know much less about such asymmetric systems than about their symmetric counterparts, and what little we know is often perplexing. For instance, recent experiments on artificial asymmetric membranes found them to be much stiffer than their cognate symmetric counterparts. In this paper we discuss the interplay between lipid asymmetry and a difference in individual leaflet tension, arguing that their intricate coupling is responsible for some of the observed phenomena, in particular an increase in membrane rigidity. We also show that the ubiquity of cholesterol, a molecule that can rapidly transition between leaflets, does not automatically eliminate a tension difference between them.

INTRODUCTION

Lipid membranes are indispensable in all domains of life. Especially in eukaryotes their ability to dynamically compartmentalize cells into functionally distinct organelles and to coordinate the flow of matter and information between those (as well as the environment) through finely orchestrated remodeling events (1) occupies many branches of cell biology (2–4).

From a materials point of view, biomembranes are self-assembled two-dimensional fluid bilayers comprising many types of lipids and proteins. On scales only mildly exceeding their thickness, they behave with astonishing accuracy like curvature elastic surfaces (5), which enables a differential geometric description that is both efficient and elegant (5–10).

Looking beyond *shape*, a biomembrane's *lipid composition* is increasingly recognized as a fundamental degree of freedom responsible for many of its functions: lipid bilayers do not just passively solubilize membrane proteins, as initially posited in the fluid mosaic model (11); they can affect protein function (12, 13), and even laterally organize membranes into compositionally distinct "rafts" (14–17). While the thermodynamic nature of these "domains" remains debated (18–23), their lateral extension is generally agreed-upon: several tens of nanometers. This exceeds membrane thickness by about an order of magnitude, which renders rafts mesoscopic environments that are not just chemically but also *elastically* distinct, thereby entangling composition with geometry.

Equally well known, but much less studied, is the fact that biomembranes are also compositionally *asymmetric*: even if we ignore the proteins, a bilayer's lipid makeup differs across the two leaflets (24–28). In fact, even if we ignore the proteins *and* the lipids, different solution conditions across

the separating membrane suffice to effectively *induce* a bilayer asymmetry, often with consequences identical to explicit lipid asymmetry (29–33).

To be clear, the dearth of biophysical research into compositionally asymmetric membranes does not reflect a lack of importance. Rather, until very recently it was essentially impossible to artificially create well-controlled asymmetric model membranes, in which the consequences of asymmetry could be explored while sidestepping many of the confounding factors present in living systems. But this has changed with the advent of two preparation techniques: the *phase transfer protocol* (34–37), in which vesicles are essentially assembled "one monolayer at a time", and the *lipid exchange protocol* (38–41), in which lipids on the outside of a vesicle are partially replaced by other ones that are loaded into a soluble exchange agent, typically methyl-β-cyclodextrin.

Recent experimental work on asymmetric membranes has largely focused on optimizing these protocols and exploring novel applications. For instance, the phase transfer protocol has been used for cargo compartmentalization (42, 43) and in synthetic biology (44–49). Less emphasis has been placed on probing the materials properties of these systems, even though the broken up-down symmetry could have profound consequences for them. Indeed, recent experiments that measured the bending rigidity of asymmetric membranes have found that these can be more than twice as rigid as their symmetric counterparts (50, 51). This is surprising for at least two reasons. First, leaflet asymmetry obviously affects a bilayer's spontaneous curvature; but this only enters the curvature energy at the linear level, whereas the bending rigidity multiplies the *square* of the curvature and hence involves qualitatively different physics. And second, if asymmetry does not change the bending rigidity of an individual leaflet from the value it would have in a symmetric membrane, then it is hard to see why the rigidity of an asymmetric membrane would not be the average rigidity of the two corresponding symmetric bilayers.

In this paper we show that leaflet asymmetry can indeed affect a bilayer's resistance to bending. However, we propose that this does not come about because asymmetry somehow breaks the additivity of individual monolayer rigidities. We instead argue that monolayers in asymmetric membranes generally differ in their physical characteristics from those in symmetric bilayers. Specifically, we show that asymmetric membranes constitute (at least) a *one-parameter non-equilibrium family of states* in which spontaneous curvature can be traded for *differential stress*—a term we propose to describe a situation in which the difference between the lateral tensions of the two leaflets does not vanish. Indeed, we argue that it is this differential stress that is responsible for stiffening. When experimentally preparing such membranes, the balance point between composition- and stress-asymmetry likely depends on both thermodynamic and kinetic details of the formation protocol. With the help of coarse-grained molecular dynamics simulations (using the MARTINI model (52, 53)), we show that membranes may stiffen beyond some minimum differential stress; in fact, we show that terms beyond quadratic order become noticeable in the energy functional. We will explain why this scenario is compatible with the null-result in the control presented in Ref. (50), where symmetric membranes created via the phase transfer protocol did not display any stiffening. We will also argue that the presence of a lipid species that can rapidly transition between leaflets (such as cholesterol) does not automatically eliminate a bilayer's differential stress. Hence, our main conclusions hold beyond the case of simple model system; they are relevant for actual biomembranes, which are generally asymmetric but may contain a very sizable fraction of cholesterol.

Our findings have implications beyond the opening question of what the rigidity of an asymmetric membrane is. They also emphasize that the very notion of an asymmetric membrane is more subtle: we need to know more than the two leaflet compositions—namely: the differential stress—in order to fully classify its state, and this information may profoundly affect its emergent elastic properties. This not only matters for the above described strategies to purposefully engineer asymmetric membranes (34–40), but also for more common vesicle preparation techniques that were recently shown to inadvertently induce asymmetry (54), or for the question how to choose the area per lipid when simulating asymmetric membranes. Ultimately, we wish to invite a new view on actual biological membranes, which are known to be highly compositionally asymmetric, but for which the possibility of an accompanying stress asymmetry is not yet routinely deliberated, let alone that this could significantly affect their elastic properties.

METHODS

Coarse-grained simulations

We used the coarse-grained (CG) MARTINI model of lipids (52) to represent membranes, and specifically worked with the following four glycero-phosphocholine-lipids: DLPC (1,2-dilauroyl-*sn*-glycero-3-phosphocholine), which has two fully saturated C12 chains; DPPC (dipalmitoyl-*sn*-glycero-3-phosphocholine), which has two fully saturated C16 chains; POPC (1-palmitoyl-2-oleoyl-*sn*-glycero-3-phosphocholine), which has a saturated C16 *sn1*-chain and a singly (cis-)unsaturated C18 *sn2*-chain; and finally DLiPC (dilinoleoyl-*sn*-glycero-3-phosphocholine), a lipid with two doubly (cis-)unsaturated C18 chains. Since MARTINI cannot properly distinguish between 16 or 18 carbons, the latter lipid is typically referred to as DIPC in the MARTINI lipidome, and we will do so, too.

Some of our simulations also contain additional cholesterol. While this lipid has been part of the original MARTINI suite (52), its parametrization was known to have numerical stability issues (due to the rigid ring structure) and exhibited several physical shortcomings; for instance, it failed to preserve fluidity of liquid-ordered domains (55, 56). These issues

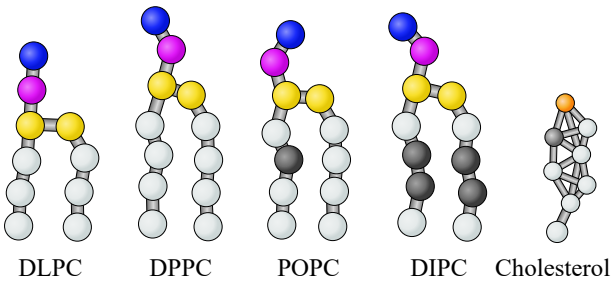

Figure 1: Illustration of the MARTINI versions of the four phospholipids and cholesterol used in this paper. The different bead colors represent: choline group (blue); phosphate group (magenta); glycerol backbone (yellow); C_4H_8 hydrocarbon repeat with single bonds (light gray); C_4H_6 hydrocarbon repeat with a cis double bond (dark gray). In the cholesterol figure, the small white beads are smaller versions of the hydrocarbon beads, the gray bead is slightly more polar, and the orange bead is the hydroxyl group.

were successfully addressed in a recent reparametrization by Melo *et al*. (57). Unfortunately, their new force field relies on virtual sites, which are not supported in the present version of GROMACS-LS (58, 59) (the package we use to calculate the lateral stress profile—see below). We hence employed a revision of the Melo force field, created by Ingólfsson (60), which strives to capture the improvements achieved in Ref. (57) without the need for virtual sites.

Fig. 1 illustrates the four phospholipids we use, together with the cholesterol model. For completeness, we recall that water is modeled explicitly with CG beads, each of which represents four atomistic water molecules.

To run the simulations, we employed GROMACS 5.1 (61, 62), using a time step of $\delta t = 20\,\mathrm{fs}$ and a 1.4 nm Verlet cutoff neighbor list updated every 10 steps. Cutoffs for Lennard-Jones and Coulomb interactions were set to their standard value of 1.2 nm, and the relative dielectric constant was set to $\epsilon_\mathrm{r} = 15$. A Berendsen thermostat (63) was used with a time constant $\tau_T = 1\,\mathrm{ps}$ to fix the temperature at $T = 300\,\mathrm{K}$ (for all our simulations). If we needed constant pressure conditions along some coordinate direction i, we used a Berendsen barostat (63) with reference pressure $P_i = 1\,\mathrm{bar}$, time constant $\tau_P = 3\,\mathrm{ps}$, and isothermal compressibility $\kappa_T = 3\times10^{-5}\,\mathrm{Pa}$.

The coarse-grained nature of MARTINI tends to speed up the dynamics, and MARTINI times are often scaled by an additional factor of 4 to account for this. We do *not* follow this practice in this paper and instead quote unscaled bare times.

Determining various observables

Bending rigidity

We measured the curvature modulus κ of simulated lipid membranes by buckling them (64–66). Briefly, we set up an anisotropic cuboid box with a dimension L_x along which we then buckle the membrane. This length exceeds both the box and membrane width L_y (which is fixed) as well as the box height L_z (which adjusts to the external pressure) by a factor of around 6 (see Table. 2 for the actual simulation parameters). We first determined the zero-tension relaxed rest length L of the membrane by also creating constant pressure conditions along the x-direction and measuring the corresponding expectation value of the box length: $L = \langle L_x\rangle_{\Sigma=0}$. We then buckle the membrane along x by imposing a fixed box-length $L_x < L$, which corresponds to a dimensionless buckling strain

$$\gamma = \frac{L - L_x}{L}\,. \tag{1}$$

The force $f_x(\gamma)$ per unit length along the x-direction (the so-called "stress-strain-relation") is measured from

$$f_x(\gamma) = \big[P_x(\gamma) - P_z\big]L_z\,, \tag{2}$$

and assuming quadratic curvature elasticity, it can be expressed as a series expansion in γ (65):

$$f_x(\gamma) = \kappa\left(\frac{2\pi}{L}\right)^2\left\{1 + \frac{1}{2}\gamma + \frac{9}{32}\gamma^2 + \frac{21}{128}\gamma^3 + \cdots\right\}\,. \tag{3}$$

Once membranes exhibit a sufficiently large stress-asymmetry between the leaflets, we found it necessary to extend this theory to permit for curvature softening, as previously used by Diggins *et al*. to quantitatively model the significant deviations from conventional curvature elasticity found in gel-phase membranes (66). Briefly, the quadratic curvature elastic energy density of $\frac{1}{2}\kappa K^2$ (where K is the total curvature, *i. e*. the sum of the two principal curvatures) is replaced by the softened expression

$$e(K) = \kappa\ell^{-2}\big[\sqrt{1 + K^2\ell^2} - 1\big]\,, \tag{4}$$

where the new material parameter ℓ is a cross-over length that indicates below which curvature radius softening sets in. This empirical functional has the properties that (*i*) it reduces to the original quadratic theory in the limit $\ell \to 0$; (*ii*) it has a negative quartic contribution $-\frac{1}{8}(\kappa\ell^2)K^4$ that promotes softening; and (*iii*) its post-quartic terms render the complete functional bounded below—in fact, convex. The modified stress-strain relation for Eqn. (4) is (66)

$$\begin{aligned} f_x(\gamma,\delta) =& \kappa\left(\frac{2\pi}{L}\right)^2\left\{1 + \frac{1}{2}\Big(1 - 3\delta^2\Big)\gamma\right. \\ &+ \frac{3}{32}\Big(3 - 14\delta^2 + 31\delta^4\Big)\gamma^2 \\ &\left.+ \frac{1}{128}\Big(21 - 129\delta^2 + 447\delta^4 - 779\delta^6\Big)\gamma^3 + \cdots\right\}\,, \end{aligned} \tag{5}$$

where $\delta = 2\pi\ell/L$ is a dimensionless smallness (or "softening") parameter: $\delta \to 0$ implies $\ell \to 0$ and reduces this more complicated expression to the simpler one from Eqn. (3). We always used Eqn. (5) to fit the stress-strain-relation measured in our simulations (using the parameters κ and δ); finding $\delta = 0$ within error bars indicates that the membrane exhibits conventional curvature elasticity.

Stress profile and associated observables

We used the GROMACS-LS package (58, 59) to calculate the lateral stress profile $\sigma_0(z)$ of a bilayer spanned in the xy-plane. Briefly, this stress is defined as

$$\sigma_0(z) = P_{zz}(z) - \frac{1}{2}\big[P_{xx}(z) + P_{yy}(z)\big] \,, \tag{6}$$

where the $P_{ii}(z)$ are the diagonal components of the local pressure tensor in a thin slice at position z. For reasons of mechanical stability $P_{zz}(z)$ must actually be constant (67), which is a good first test for correctness and convergence. To avoid fluctuation blurring of $\sigma_0(z)$, it is best to simulate small membranes with only $O(100)$ lipids (68).

The tension per leaflet, $\Sigma_\pm$, is the integral of $\sigma_0(z)$ over the respective leaflet, ranging from the bilayer midplane into the bulk water phase. Since $\sigma_0(z)$ rapidly decays to zero for z values outside the membrane, the precise location of the outer boundary is immaterial, provided it is sufficiently far away from the membrane:

$$\Sigma_\pm = \int_0^{+\cdots} \mathrm{d}z\; \sigma_0(\pm z) \,, \tag{7}$$

where $z = 0$ marks the location of the midplane. Notice that for asymmetric membranes the latter need not coincide with the z-coordinate of the membrane's center of mass, which is the location to which GROMACS-LS shifts the membrane if one chooses to center it. The integral itself can be easily done numerically by a Gaussian quadrature of the local stresses calculated by GROMACS-LS for each individual z-bin.

Another observable of interest is the first moment of the stress profile, the torque density $\mathcal{T}$ (31):

$$\mathcal{T} = \int_{-\cdots}^{+\cdots} \mathrm{d}z\; \sigma_0(z)\, z \,, \tag{8}$$

because in the absence of both net and differential stress it is connected to the bilayer's spontaneous materials curvature $K_{0\mathrm{b}}$ (see Eqn. (13) below) (31, 69–71):

$$\kappa K_{0\mathrm{b}} = -\mathcal{T} \qquad \text{if } \Sigma_\pm = 0 \,. \tag{9}$$

Orientational order parameter

A standard measure for assessing the degree of lipid orientational order is the so-called P_2 order parameter, defined as

$$P_2 = \langle \mathrm{P}_2(\cos\vartheta_i)\rangle = \frac{1}{2}\left(3\left\langle\cos^2\vartheta_i\right\rangle - 1\right) \,, \tag{10}$$

where $\mathrm{P}_2(x)$ is the second Legendre polynomial, and ϑ_i is the angle between the orientation of a lipid i and the average membrane normal (here: the z-direction). The average is taken over all lipids in a membrane, or all lipids in one of the leaflets. A lipid's orientation is defined through the vector pointing from the midpoint between the two tail-endbeads to the head bead. Larger values of P_2 indicate stronger lipid alignment; $P_2 = 1$ indicates perfect alignment, $P_2 = 0$ signals completely random directions, and $P_2 = -\frac{1}{2}$ occurs when lipids align perpendicularly to the chosen axis.

Specific heat

As a common means to probe for phase transitions, we also calculated the isobaric specific heat c_P for a membrane (in the flat state). The classical fluctuation-response theorem teaches that c_P is proportional to the enthalpy fluctuations:

$$\frac{c_P}{k_\mathrm{B}} = \frac{\sigma_H^2}{N(k_\mathrm{B}T)^2} \,, \tag{11}$$

where $k_\mathrm{B}T$ is the thermal energy, $\sigma_H^2 = \langle H^2\rangle - \langle H\rangle^2$ is the variance of the enthalpy $H = E + PV$, and N the total number of particles, which in our case is the total number of beads.

Two small comments are in order. First, even though we simulate our aqueous membrane systems at fixed pressure, their tiny compressibility renders the difference between the isobaric and isochoric specific heat negligible—we find $(c_P - c_V)/k_\mathrm{B} \sim O(10^{-4})$. And second, it is well known that the Berendsen thermostat does not precisely reproduce the canonical ensemble, since it suppresses fluctuations in the kinetic energy (62). For us this matters only insofar as the value of c_P calculated via Eqn. (11) will miss part of its kinetic contribution (we found it to be about $0.75k_\mathrm{B}$ too small). However, the impact on the configurational degrees of freedom vanishes like $1/N$, and so the thus calculated c_P is still an excellent indicator for phase transitions, which are driven by the potential contribution to the Hamiltonian.

RESULTS—THEORY

Asymmetry and spontaneous curvature

We start with a general review of the connection between bilayer asymmetry, spontaneous curvature, and differential stress. While this subject has been discussed in a number of recent publications (31, 32, 72–74), we nevertheless wish to revisit the key ideas, because some of the implications, especially when both spontaneous curvature and differential stress are present, appear not to have been explicitly spelled out yet. As a graphical summary, Figure 2 illustrates the main ingredients that enter this discussion.

From two individual monolayers to a single bilayer

Consider a compositionally asymmetric membrane whose two leaflets are characterized by monolayer bending rigidities ($\kappa_{\mathrm{m}+}$, $\kappa_{\mathrm{m}-}$) and spontaneous curvatures ($K_{\mathrm{m}+}$, $K_{\mathrm{m}-}$). In what follows we will use the subscript "m" to indicate monolayer observables and labels "+" and "−" for the upper and lower leaflet, respectively. Bilayer quantities will follow the same sign convention as the upper leaflet. To assist with parsing the subsequent theoretical part, we collect a list of the more frequent symbols and notations in a Glossary at the end of the paper.

If we impose a weak curvature K, permit the two leaflets to slide past each other, ensure that they are individually tensionless, and ignore (here, and in all following discussions)

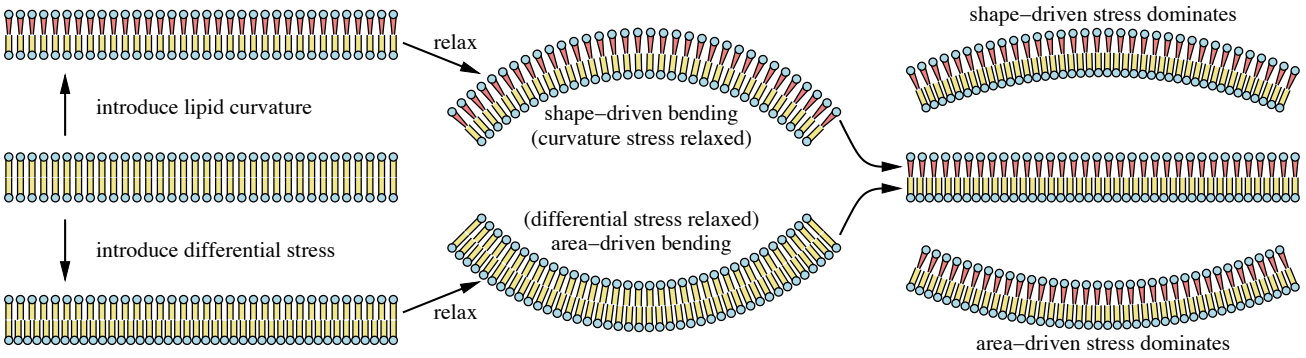

Figure 2: Illustration of the interplay between a spontaneous curvature K_{0b} driven by lipid shape and a spontaneous curvature K_{0s} driven by area strain. An initially flat and relaxed membrane can be asymmetrically stressed either by a leaflet imbalance of lipid shape, or a leaflet imbalance in the area density. Such membranes relax by assuming a shape- or area-driven spontaneous curvature. When both effects occur simultaneously (see right hand side), the resulting spontaneous curvature K_0 arises as the balances expressed in Eqn. (18), which can include an asymmetric, flat, and differentially stressed membrane as a special case.

the topological Gaussian contribution, then the energy density comprises only two bending terms and is given by

$$e_0(K) = \frac{1}{2}\kappa_{m+}(K - K_{m+})^2 + \frac{1}{2}\kappa_{m-}(K + K_{m-})^2 \,. \qquad (12)$$

The first term captures the upper leaflet, the second term the lower one, and the swapped sign of K_{m-} allows for the fact that the lower leaflet curvature is flipped with respect to the upper one.

Minimizing this energy yields the bilayer's spontaneous materials curvature K_{0b} at which the net bending stress vanishes (hence the subscript "b"), namely, the *rigidity-weighted difference* of the two spontaneous leaflet curvatures:

$$\left.\frac{\partial e_0(K)}{\partial K}\right|_{K=K_{0b}} = 0 \quad \Rightarrow \quad K_{0b} = \frac{\kappa_{m+}K_{m+} - \kappa_{m-}K_{m-}}{\kappa_{m+} + \kappa_{m-}} \,. \qquad (13)$$

Using it, the bending energy can be written as

$$e_0(K) = \text{const.} + \frac{1}{2}\kappa(K - K_{0b})^2 \,, \qquad (14)$$

where the bilayer curvature modulus is the sum of the monolayer curvature moduli, $\kappa = \kappa_{m+} + \kappa_{m-}$, and the constant can be absorbed into the net tension.

Since the individual $K_{m\pm}$ can be large, this can be true for K_{0b}, too. As a numerical example, let us look at the membrane parameters reported in Table 1. For an asymmetric $\frac{\text{DOPC}}{\text{POPC}}$ membrane we get $K_{0b} \approx -0.017\,\text{nm}^{-1}$; a sphere with this curvature would have a radius of $R_{0,b} = 2|K_{0b}^{-1}| \approx 120\,\text{nm}$, a typical size for a large unilamellar vesicle (LUV) or many intracellular transport vesicles. But if we take a $\frac{\text{DOPC}}{\text{DOPE}}$ membrane, we get $K_{0b} \approx 0.1\,\text{nm}^{-1}$, or a curvature radius of $R_{0,b} = 2|K_{0b}^{-1}| \approx 20\,\text{nm}$, typical for small unilamellar vesicles (SUV) or synaptic vesicles.

Table 1: Material parameters for a few standard lipid systems, determined from atomistic simulations (75). The length d is the distance between the mean C_2 carbon position in the two leaflets and is a measure of the membrane's hydrophobic thickness.

lipid	T [K]	κ_m [pN nm]	K_m [nm^{-1}]	d [nm]
DOPC	298	59	−0.0714	2.737
POPC	303	66	−0.0317	2.752
DOPE	298	59	−0.2703	2.996

Varieties of metastability

Even a bilayer satisfying $K = K_{0b}$ is generally *not* in an equilibrium state, for the underlying asymmetric lipid distribution can relax into a symmetric one when lipids flip-flop between leaflets. However, the associated time scales tend to be very long, and even though the matter is still actively debated, times between many hours and many days have been repeatedly measured for not-too-short lipids in unsupported membranes (see Ref. (76) for a recent review). This means that on time scales much shorter than the typical flip-flop time, the asymmetric distribution can be treated as a metastable equilibrium.

But if so, then *other* metastable states rendered possible by slow flip-flop must also be considered—chiefly among them *differentially stressed* states in which the mechanical tensions $\Sigma_\pm$ in the two leaflets are unequal (31, 77–79). The easiest situation to contemplate, and to which we will restrict here, is one in which the *net* bilayer tension $\Sigma = \Sigma_+ + \Sigma_-$ vanishes, but in which the two leaflets individually exhibit a nonzero tension that is equal in magnitude but opposite in sign: one layer being subject to tensile stress (positive tension), the other one subject to compressive stress (negative tension).

Spontaneous curvature under differential stress

Like bimetallic strips, differentially stressed membranes can relax by bending. We will assume that this happens as illustrated in Fig. 2; specifically, we demand that the two leaflets share a common midplane before and after a change in curvature. Assume therefore that at some particular spontaneous curvature $K_{0\mathrm{s}}$ the differential area strain vanishes (hence the additional subscript "s"). Notice that unlike $K_{0\mathrm{b}}$, which by Eqn. (13) is a material parameter, $K_{0\mathrm{s}}$ instead characterizes the lipid packing in the two leaflets, which is likely set by whatever kinetics process creates the bilayer.

Using the parallel surface theorem (10, 80), it is easy to see that changing the curvature from $K_{0\mathrm{s}}$ to K, we create a *local* differential area strain

$$\gamma_\pm(K) = \pm(K - K_{0\mathrm{s}})z_\pm + O(z_\pm^2) \tag{15}$$

in leaflet reference surfaces a distance $z_\pm$ away from the bilayer midplane. But since individual leaflets can slide, the physically meaningful strain is not the local one, but the one distributed over the whole membrane. This yields a *nonlocal* curvature elastic energy density that has been included in numerous membrane models (81–86)

$$e_{\mathrm{nl}} = \frac{1}{2}K_{A,\mathrm{m}+}\gamma_+^2(\bar{K}) + \frac{1}{2}K_{A,\mathrm{m}-}\gamma_-^2(\bar{K}) \tag{16a}$$

$$= \frac{1}{2}\kappa_{\mathrm{nl}}(\bar{K} - K_{0\mathrm{s}})^2\,, \tag{16b}$$

which quadratically penalizes the deviation of the surface-averaged curvature

$$\bar{K} = \frac{1}{A}\int_{\mathcal{S}} \mathrm{d}A\; K \tag{16c}$$

from the differential stress curvature $K_{0\mathrm{s}}$ with the nonlocal bending rigidity[1]

$$\kappa_{\mathrm{nl}} = K_{A,\mathrm{m}+}z_+^2 + K_{A,\mathrm{m}-}z_-^2 \overset{*}{\approx} K_A z_0^2\,. \tag{16d}$$

At "$*$" we made the additional simplifying assumption that $z_+ = z_- \equiv z_0$ and defined the bilayer area expansion modulus $K_A = K_{A,\mathrm{m}+} + K_{A,\mathrm{m}-}$.

If we choose $z_\pm$ to be the neutral surfaces (*i. e.*, the surface at which bending and stretching deformations decouple (87)), then—by definition—the associated elastic energy (16b) of stretching or compression simply adds to the curvature energy from Eqn. (12). Up to a constant, which we can subsume in the net tension, this leads to the total energy density

$$e_{\mathrm{tot}}(K, \bar{K}) = \frac{1}{2}\kappa(K - K_{0\mathrm{b}})^2 + \frac{1}{2}\kappa_{\mathrm{nl}}(\bar{K} - K_{0\mathrm{s}})^2\,. \tag{17a}$$

These are two quadratic curvature terms, a local and a nonlocal one, for which $K_{0\mathrm{b}}$ and $K_{0\mathrm{s}}$ are the respective spontaneous curvatures. The first term is traditionally referred to as the "spontaneous curvature model" (5), and the second as the "area difference elasticity" model (86). These are usually viewed as two alternative models for describing curvature elasticity in the presence of an asymmetry that prefers a nonzero bilayer curvature. Notice, though, that not only do these two models describe conceptually very different origins of such an asymmetry, they also describe different elastic energies: bending versus stretching. As such, it is legitimate to write the total elastic energy as their sum.

If, for simplicity, we specialize to constant mean curvature surfaces (such as spheres, cylinders, or unduloids), for which $K \equiv \bar{K}$, and again ask when the overall curvature energy is minimized, we get

$$\left.\frac{\partial e_{\mathrm{tot}}(K,K)}{\partial K}\right|_{K=K_0^\star} = 0 \quad\Rightarrow\quad K_0^\star = \frac{\kappa K_{0\mathrm{b}} + \kappa_{\mathrm{nl}}K_{0\mathrm{s}}}{\kappa + \kappa_{\mathrm{nl}}}\,. \tag{18}$$

A new spontaneous curvature, $K_0^\star$, once again arises as a weighted mean—this time of the curvatures associated with optimal bending, $K_{0\mathrm{b}}$, and optimal stretching, $K_{0\mathrm{s}}$, for which κ and κ_{nl} are the respective weighting factors.[2]

In the balance condition (18) the stretching penalty should dominate, because bending is the softer degree of freedom, and so we should expect $\kappa/\kappa_{\mathrm{nl}}$ to be small. Indeed, from the polymer brush model (88) we know that a reasonable approximation for a bilayer's bending rigidity is $\kappa \approx K_A d_{\mathrm{h}}^2/24$, where d_{h} is the bilayer's hydrophobic thickness (typically about 2/3 of its total width d). Since furthermore $z_0 \approx d_{\mathrm{h}}/2$ (89, 90) and $\kappa_{\mathrm{nl}} \approx K_A z_0^2$, we find $\kappa/\kappa_{\mathrm{nl}} \approx 1/6$.

A one-parameter family of asymmetric membranes

Despite being energy minimized, the curvature-relaxed state from Eqn. (18) with $K = K_0^\star$ exhibits a differential strain $\gamma_\pm = \pm(K_0^\star - K_{0\mathrm{s}})z_\pm$ and a concomitant differential stress

$$\Sigma_\pm = K_{A,\mathrm{m}\pm}\gamma_\pm \approx \pm\frac{\kappa}{2z_0}\frac{K_{0\mathrm{b}} - K_{0\mathrm{s}}}{1 + \kappa/\kappa_{\mathrm{nl}}}\,. \tag{19}$$

Only in the special case $K_{0\mathrm{s}} = K_{0\mathrm{b}}$ does this stress vanish. But we can imagine other scenarios—for instance a flat membrane in which the differential stress exactly cancels the bending moment induced by the spontaneous curvature $K_{0\mathrm{b}}$; in other words, *an asymmetric bilayer that nevertheless has a vanishing spontaneous curvature*: $K_0^\star = 0$. From Eqn. (18) this implies $K_{0\mathrm{s}} = -(\kappa/\kappa_{\mathrm{nl}})K_{0\mathrm{b}}$ and hence

$$\Sigma_\pm(K_0^\star = 0) = \pm\frac{\kappa K_{0\mathrm{b}}}{2z_0}\,. \tag{20}$$

[1] A similar non-local bending rigidity κ' is defined in Refs. (84, 86), however with a curious extra factor of π, so that we have $\kappa_{\mathrm{nl}} = \pi\kappa'$.

[2] Incidentally, up to a constant the energy has the form $\frac{1}{2}C(K - K_0^\star)^2$ with some "effective" bending rigidity $C = \kappa + \kappa_{\mathrm{nl}}$. This is not surprising, since Eqn. (17a) essentially describes two springs in parallel. However, C should *not* be interpreted as a local bending rigidity, since the derivation relied on constant mean curvature surfaces in order to trivially combine the local and the nonlocal bending part.

Physically, the sign can be understood as follows: if from a spontaneous curvature point of view we have $K_{0\mathrm{b}} > 0$, so that the upper leaflet is convex, it also needs to be under a positive tension to pull it back into a flat state. Using the numbers discussed before, a $\frac{\mathrm{DOPC}}{\mathrm{POPC}}$ membrane in such a state would then end up with a noticeable differential stress of $|\Sigma_\pm| \approx 0.8\,\mathrm{mN/m}$, while for a $\frac{\mathrm{DOPC}}{\mathrm{DOPE}}$ membrane we get $|\Sigma_\pm| \approx 4\,\mathrm{mN/m}$, which is very large.

Of course, the two particular states of stress just discussed are simply special cases in a *continuum of states* that can be parametrized by $K_{0\mathrm{s}}$, or (at least for $K_{0\mathrm{b}} \neq 0$) by the dimensionless stress-curvature parameter

$$\alpha_{\mathrm{sc}} := \frac{1 - K_{0\mathrm{s}}/K_{0\mathrm{b}}}{1 + \kappa/\kappa_{\mathrm{nl}}}\,, \tag{21}$$

which labels states with the differential stress

$$\Sigma_\pm(\alpha_{\mathrm{sc}}) = \pm\alpha_{\mathrm{sc}} \times \frac{\kappa K_{0\mathrm{b}}}{2z_0}\,. \tag{22}$$

Our two cases from above correspond to $\alpha_{\mathrm{sc}} = 0$, a membrane that assumes its "materials-based" curvature $K_{0\mathrm{b}}$ and is free of differential stress, and $\alpha_{\mathrm{sc}} = 1$, a flat membrane that exhibits differential stress. Since α_{sc} can vary continuously, asymmetric membranes really constitute (at least) a *one-parameter family of metastable states*, and for this reason *they are insufficiently characterized by their compositional asymmetry alone*. Stated differently, there is no particular value for the differential stress (say, zero) that is the "right" one, unless there is some independent argument that would permit reducing this one-parameter family of legitimate states to that special case.

Residual differential stress

The interplay between asymmetry and tension in lipid bilayers gives rise to another intriguing issue, recently identified in simulations (91, 92): the state point at which the areas per lipid in each leaflet of an asymmetric membrane agree with those in their tensionless symmetric counterparts need not coincide with the point where the differential stress vanishes. This is of practical relevance: if one wishes to simulate asymmetric membranes whose leaflets are individually tensionless (recall: a possible choice, even though not the only valid one), then it is insufficient to match the specific lipid areas in each leaflet to those in the cognate symmetric bilayers. (Ref. (91) proposes a method to correct for this, if zero tension is indeed what one wants.) Let us attempt to rationalize this empirical finding within the framework developed in the preceding sections.

Taking the specific area from simulations of a flat symmetric membrane is equivalent to imposing $K_{0\mathrm{s}} = 0$; but the bending torque that arises in the asymmetric case induces a nonzero spontaneous bilayer curvature and associated differential stress, given by Eqns. (18) and (19), respectively (while setting $K_{0\mathrm{s}} = 0$ in both equations). However, for such a membrane to be spontaneously flat, it would need to be subject to the slightly larger differential stress from Eqn. (20). The difference between these two is

$$\Delta\Sigma_\pm = \Sigma_\pm(K_0^\star = 0) - \Sigma_\pm(K_{0\mathrm{s}} = 0) \tag{23a}$$

$$= \pm\frac{\kappa K_{0\mathrm{b}}}{2z_0}\,\frac{1}{1 + \kappa_{\mathrm{nl}}/\kappa}\,. \tag{23b}$$

In other words, forcing the membrane to be planar requires this much more differential stress. Of course, we cannot "summon" additional intrinsic stress; but spanning a membrane patch into a simulation box amounts to *externally* imposing the *negative* of this differential stress via the applied periodic boundary conditions. This results in the observed *residual differential stress* of

$$\Sigma_\pm^{(\mathrm{res})} = -\Delta\Sigma_\pm = \mp\frac{\kappa K_{0\mathrm{b}}}{2z_0}\,\frac{1}{1 + \kappa_{\mathrm{nl}}/\kappa} \approx \mp\frac{\kappa K_{0\mathrm{b}}}{14 z_0}\,, \tag{24}$$

where in the last step we used the previously discussed estimate $\kappa_{\mathrm{nl}}/\kappa \approx 6$.

Notice that $\Sigma_\pm^{(\mathrm{res})}$ and $K_{0\mathrm{b}}$ strive to bend the membrane in the same direction. Hence, the *sign* of a membrane's residual differential stress conforms to what we would expect based on its spontaneous curvature. But its *magnitude* does not: it is smaller than the torque couple associated stress $\mp\kappa K_{0\mathrm{b}}/2z_0$ by the sizable factor $(1 + \kappa_{\mathrm{nl}}/\kappa)$. This shows that the residual differential stress does *not* merely embody a bilayer's spontaneous materials curvature but instead reflects a more subtle balance between bending and stretching—as quantified by the difference between $K_0^\star$ and $K_{0\mathrm{s}}$. Notice in particular that it incorporates a specific choice of boundary- and initial conditions (namely: a simulation box and $K_{0\mathrm{s}} = 0$).

If we wanted to calculate $\kappa K_{0\mathrm{b}}$ as the first moment of the stress profile belonging to the area-matched membrane, using Eqns. (8) and (9), we encounter the slight complication that this system has differential stress and so Eqn. (9) does not strictly apply, as there are now *two* physical sources of spontaneous curvature. However, we can self-consistently correct for that. If we denote the actual stress profile by $\sigma(z)$ and assume that the residual stress $\Sigma_\pm^{(\mathrm{res})}$ acts approximately evenly over the thickness $d_{\mathrm{m}\pm}$ of each leaflet, then the profile with the residual differential stress removed is given by

$$\sigma_0(z) = \sigma(z) - \begin{cases} \Sigma_+^{(\mathrm{res})}/d_{\mathrm{m}+} & 0 < z < d_{\mathrm{m}+} \\ \Sigma_-^{(\mathrm{res})}/d_{\mathrm{m}-} & d_{\mathrm{m}+} < z < 0 \end{cases}\,. \tag{25}$$

Combining this "de-stressing" correction with Eqns. (8), (9), and (24) then leads to

$$\Sigma_\pm^{(\mathrm{res})} = \pm\frac{\mathcal{T}}{2z_0(1 + \kappa_{\mathrm{nl}}/\kappa) + d/2} \approx \pm\frac{\mathcal{T}}{15.5\,z_0}\,, \tag{26}$$

where the torque density $\mathcal{T}$ is the first moment of the *actual* stress profile $\sigma(z)$ (*i. e.*, the one that has a differential stress) and $d = d_{\mathrm{m}+} + d_{\mathrm{m}-}$ is the bilayer thickness. Also, since the neutral surface can typically be found one-third of the

distance along the hydrocarbon chain from the polar head group (89), meaning $z_0 \approx \frac{2}{3}d_\mathrm{m}$, we estimated $d = 2d_\mathrm{m} \approx 3z_0$ in the last step. Had we alternatively assumed that the residual stress localizes at the neutral surface, and accordingly subtracted $\Sigma_\pm^{(\mathrm{res})}\delta(z \mp z_0)$ from each bare leaflet stress, the extra term "$+d/2$" in the denominator of Eqn. (26) would have been replaced by "$+z_0$", and the numerical value in the last expression then drops from 15.5 to 15. The precise functional form of the residual stress is dictated by the z-dependence of the area expansion moduli $K_{A,\mathrm{m}\pm}(z)$ (93), but our two limiting cases (entirely even vs. delta-localized) yield fairly similar results. In fact, the change with respect to Eqn. (24) is minor: simply replacing $\kappa K_{0\mathrm{b}}$ with $-\mathcal{T}$ gives an answer only about 10% too big. This is almost certainly less than the error incurred by empirical estimates such as $\kappa_\mathrm{nl}/\kappa \approx 6$ or $d = 3z_0$.

To test Eqns. (24) or (26), one would have to measure both the residual differential stress $\Sigma_\pm^{(\mathrm{res})}$ as well as either the spontaneous materials curvature $K_{0\mathrm{b}}$ or the torque density $\mathcal{T}$. Luckily, all of these are reported—over a range of spontaneous bilayer curvatures—in a recent paper by Miettinen and Lipowsky (92): For their "lollipop-like" model of GM1, their Fig. 5 shows that $\kappa K_{0\mathrm{b}} \approx 0.15\phi\,\mathrm{pN}$ for a membrane that contains a fraction ϕ of GM1 lipids only in its upper leaflet (hence giving the membrane a positive spontaneous curvature). Estimating $z_0 \approx 1.5\,\mathrm{nm}$ from their Fig. 1, our Eqn. (26) then predicts residual single leaflet tensions of $\Sigma_\pm^{(\mathrm{res})} \approx \mp 0.0065\phi\,\mathrm{mN/m}$, or a difference between these of $-0.013\phi\,\mathrm{mN/m}$. For comparison, their Fig. 3 reports about $-0.016\phi\,\mathrm{mN/m}$ for this difference, which agrees fairly well with our estimate.

Partial flip-flop equilibrium: the role of cholesterol

While the relaxation times for asymmetric lipid compositions are very long for typical charged or zwitterionic phospholipids, cholesterol is believed to flip-flop several orders of magnitude faster (76, 94). Hence, there exists a physiologically relevant time window within which phospholipids maintain their compositional asymmetry, while the cholesterol distribution is equilibrated between the leaflets. How does this change our considerations for spontaneous curvature and differential stress?

A comprehensive discussion of this situation goes beyond the scope of the present paper, since it would require a much more careful treatment of the equation of state of lipid-cholesterol mixtures, as for instance recently given by Allender *et al*. (74). But there is one important point we wish to emphasize: even if the cholesterol distribution can relax, this does *not* automatically imply that any previously existing differential stress will decay to zero, in contrast to a recent claim by Miettinen and Lipowsky (92). This is because stress equilibration is not the thermodynamic condition that determines the distribution of cholesterol between the leaflets. The correct condition is equilibration of *chemical potential* (74), and this will not entail a stress relaxation, any more than the ability of water to cross a semipermeable membrane between two different osmolytes will relax the osmotic pressure.

Let us illuminate this point with a strongly simplified model. Consider a bilayer that contains $L_\pm$ lipids of type $\pm$ and specific area $a_\pm$ in its $\pm$ leaflets, and also add $N_\pm$ cholesterol molecules of specific area a to these leaflets. Making the rather crude assumption that lipid areas add, we expect an equilibrium total area $\mathcal{A}_\pm = L_\pm a_\pm + N_\pm a$ for each leaflet. Since generally $\mathcal{A}_+ \neq \mathcal{A}_-$, the membrane will be differentially stressed even at zero net tension. If the "normal" lipids stay in their leaflets, but cholesterol flip-flops to equilibrate its chemical potential (subject to the constraint $N_+ + N_- = N$), what is then the equilibrium area A, the final cholesterol distribution, and the resulting differential stress?

We propose that, for the purpose of the present argument, the relevant physics can be captured by an approximate empirical free energy that accounts for the following three major physical effects: (*i*) the partitioning free energy $g_\pm$ per cholesterol molecule into the two leaflets; (*ii*) the elastic energy of leaflet stretching or compression; and (*iii*) the entropy of cholesterol's distribution between the leaflets:

$$\begin{aligned} G(A, N_+) = &-g_+N_+ - g_-N_- \\ &+ \frac{1}{2}K_{A,\mathrm{m}+}\frac{(A-\mathcal{A}_+)^2}{\mathcal{A}_+} + \frac{1}{2}K_{A,\mathrm{m}-}\frac{(A-\mathcal{A}_-)^2}{\mathcal{A}_-} \\ &+ Nk_\mathrm{B}T\big[\varphi\log\varphi + (1-\varphi)\log(1-\varphi)\big]\,, \end{aligned} \tag{27}$$

where $\varphi = N_+/N$ is the cholesterol fraction in the +-leaflet and the last line is an entropic term that measures the distribution of cholesterol between the two leaflets (which is not considered part of $g_\pm$).

The condition $\partial G/\partial A = 0$ ensures zero net tension and gives the equilibrium area $A_\mathrm{eq} = (\alpha_+/\mathcal{A}_+ + \alpha_-/\mathcal{A}_-)^{-1}$, where $\alpha_\pm = K_{A,\mathrm{m}\pm}/K_A$. Notice that deriving this condition involves only the elastic contribution (second line) to the free energy, which upon inserting it back simplifies to

$$G_\mathrm{elast}(A = A_\mathrm{eq}, N_+) = \frac{1}{2}K_A\alpha_+\alpha_-\frac{(\mathcal{A}_+ - \mathcal{A}_-)^2}{\alpha_+\mathcal{A}_- + \alpha_-\mathcal{A}_+}\,. \tag{28}$$

Since this is proportional to the square of the difference of the original leaflet areas $\mathcal{A}_\pm$, the elastic part of the free energy *by itself* is minimized when $\mathcal{A}_+ = \mathcal{A}_-$.

The cholesterol distribution now follows from equilibrating cholesterol's chemical potential between the leaflets, which is equivalent to demanding $(\partial G/\partial N_+)_{A_\mathrm{eq},N} = 0$. Unfortunately, this expression is very messy; but it simplifies considerably under the fairly good assumption that $K_{A,\mathrm{m}+} = K_{A,\mathrm{m}-}$, or $\alpha_+ = \alpha_- = \frac{1}{2}$. Expressing the cholesterol distribution via its deviation from even, $\psi := \varphi - \frac{1}{2}$, and expanding the entropy term to linear order around $\psi = 0$, we find after a short calculation

$$\psi(\Delta g, \Delta A_0, T) = \frac{\Delta g - \phi_0 K_A \Delta A_0/N}{4k_\mathrm{B}T + 2\phi_0 K_A a}\,, \tag{29}$$

with the convenient abbreviations

$$\Delta g = g_+ - g_- \,, \tag{30a}$$
$$\Delta A_0 = L_+ a_+ - L_- a_- \,, \tag{30b}$$
$$\phi_0 = Na/(L_+ a_+ + L_- a_- + Na) \,. \tag{30c}$$

These three terms signify, in turn, the partitioning free energy difference per cholesterol molecule, the leaflet area difference in the absence of cholesterol, and cholesterol's average area fraction in tensionless leaflets. The differential stress associated with this cholesterol distribution is

$$\Sigma_\pm = \left(\frac{\partial G_\pm}{\partial A}\right)_{T,A_{\mathrm{eq}},N} = \frac{1}{2} K_A \frac{\mathcal{A}_- - \mathcal{A}_+}{\mathcal{A}_- + \mathcal{A}_+} \tag{31a}$$
$$= \mp \phi_0 K_A \left(\frac{\Delta A_0}{2Na} + \psi(\Delta g, \Delta A_0, T)\right) \tag{31b}$$
$$= \mp \frac{1}{2} \phi_0 K_A \frac{\Delta A_0/Na + \Delta g/2k_\mathrm{B}T}{1 + \phi_0 K_A a/2k_\mathrm{B}T} \,. \tag{31c}$$

To elucidate the meaning of these predictions, it is instructive to examine two limiting cases. Let us first look at a situation in which both the partitioning free energy difference and entropic effects vanish (*i. e.*, $\Delta g = 0$ and $T = 0$). In this special case, Eqn. (29) simplifies to

$$\psi(\Delta g = 0, \Delta A_0, T = 0) = -\frac{\Delta A_0}{2Na} \,. \tag{32}$$

The cholesterol asymmetry is proportional to the bare-lipids area difference in the two leaflets, and it is easy to check that Eqn. (32) implies $\mathcal{A}_+ = \mathcal{A}_-$. In other words, the areas are balanced and, within the framework of our model, the differential stress vanishes exactly—as either Eqn. (31a) or Eqn. (31b) readily show.

Notice, though, that a full stress cancellation only occurs if we neglect entropic effects, because back-filling the expanded leaflet with cholesterol diverted from the compressed leaflet will imply a deviation from the true free energy minimum. Even if cholesterol prefers no leaflet over the other, entropic effects will create a partitioning shift $\Delta\psi$ away from the stress free state:

$$\Delta\psi = \psi(\Delta g = 0, \Delta A_0, T) - \psi(\Delta g = 0, \Delta A_0, T = 0) \tag{33a}$$
$$= \frac{\Delta A_0 \, k_\mathrm{B}T}{N\phi_0 K_A a^2} + O(T^2) \,, \tag{33b}$$

or

$$\frac{\Delta\psi}{\psi(\Delta g = 0, \Delta A_0, T = 0)} = -\frac{2\,k_\mathrm{B}T}{\phi_0 K_A a} + O(T^2) \,. \tag{34}$$

This expression is negative, showing that the shift always *counteracts* the cholesterol displacement from Eqn. (32) that would fully eliminate the differential stress. Hence, in the presence of entropy, stress cancellation is incomplete, even when $\Delta g = 0$.

In the general case cholesterol will of course prefer one of the two leaflets of an asymmetric membrane over the other. Let us hence look at the second limiting case, in which a finite preference Δg exists, but where the bilayer creation process achieved $\Delta A_0 = 0$, *i. e.*, a bilayer which in the absence of cholesterol harbors no differential stress. Notice that (within our model) this would stay true if we added cholesterol *evenly* to the two leaflets: $N/2$ molecules to each leaflet, or, $\psi = 0$. But if we now permit the cholesterol to flip-flop and find its true free energy minimum, we get

$$\psi(\Delta g, \Delta A_0 = 0, T) = \frac{\Delta g}{4k_\mathrm{B}T + 2\phi_0 K_A a} \,, \tag{35}$$

showing that if the +-leaflet is preferred by Δg, then a cholesterol asymmetry proportional to Δg arises. In other words: the addition of cholesterol may not only fail to fully balance the stresses, as in the previous case; it may actually *create* a differential stress that was not there in the absence of cholesterol. Notice that this is opposed by two different phenomena: first, the entropy (the first term in the denominator); and second, the fact that the emerging asymmetry creates new stresses that cost elastic energy (the second term in the denominator).

To estimate the magnitude of this asymmetry, let us take $\Delta g \approx 2\,k_\mathrm{B}T$, a recently determined partitioning free energy difference for cholesterol between a saturated stearoylsphingomyelin bilayer and an unsaturated POPC bilayer (95). Using furthermore $K_A \approx 250\,\mathrm{mN/m} \approx 60\,k_\mathrm{B}T/\mathrm{nm}^2$ (88), $a \approx 0.25\,\mathrm{nm}^2$ (96), and $\phi_0 = 20\%$, this leads to a large partitioning asymmetry of $\psi \approx 36\%$ and, from Eqn. (31c), an associated differential stress of $|\Sigma_\pm| \approx 10\,\mathrm{mN/m}$ for the parameters chosen above—a *very* large value. This is most likely outside the regime of validity of our linear expansions, but it indicates that small partitioning differences can drive large stresses.

We hasten to add that this model has many weaknesses. For instance, we assume our partitioning free energies $g_\pm$ to be independent of the cholesterol content in each leaflet. This is incorrect not just because of the obvious role played by the chemical environment; there is also an *elastic* effect: even flat membranes have bending stresses due to nonzero spontaneous curvatures $K_{\mathrm{m}\pm}$, and since $K_{\mathrm{m}\pm}$ generally depends on the cholesterol mole fraction, this creates another thermodynamic driving force, as recently emphasized by Allender *et al.* (74). An even more subtle issue is the assumption of area additivity, and the prerequisite of giving meaning to the notion of specific lipid area. This is fraught with numerous complications, because the presence of cholesterol in a bilayer changes the conformational ensemble of the host-phase lipids (97), affecting area per lipid (96, 98–101) as well as other material parameters, such as the spontaneous curvature (74, 97, 102) and the bending rigidity (103–107). In particular, addition of cholesterol can actually *contract* a membrane, leading to a negative *partial* specific area (96, 101). To do better, we need a quantitative understanding of the underlying equations of state, but this is not presently our goal.

Let us now return to the claim by Miettinen and Lipowsky that the presence of a species with a high flip-flop rate will render the individual leaflets tensionless (92). In their simulations, these authors studied an asymmetric membrane containing POPC in one leaflet, and a mixture of POPC with (two slightly different versions of) the ganglioside GM1 (the glycosphingolipid monosialotetrahexosylganglioside). Since POPC has one monounsaturated tail, and GM1 contributed with its saturated tails at most up to 25 mol% in one of the leaflets, the partitioning free energy difference Δg is likely very small. These simulations hence appear closer to the first limit discussed above, in which cholesterol fosters an (incomplete) differential stress relaxation. This is indeed what the authors find, even if the stress in question is slightly more subtle in nature (namely: a residual differential stress). However, whether cholesterol would also undo a bilayer's differential stress in the presence of a noticeable Δg cannot hence be inferred from these simulations.

RESULTS—SIMULATION

Measuring rigidities in coarse-grained simulations

We begin by measuring the bending rigidity κ of symmetric DLPC and POPC bilayers that are tensionless and hence, due to their symmetry, also free of differential stress. Our results indicate that both membranes have basically the same[3] value of κ within error bars and show only weak (albeit statistically significant) signs of curvature softening (see Tab. 2 for these and all subsequent measurement results).

Let us now investigate an asymmetric membrane in which one leaflet is pure DLPC and the other one pure POPC and first choose the specific lipid areas in each leaflet to match those in their cognate symmetric tensionless system (DLPC: $a_\ell = 0.5709(3)\,\mathrm{nm}^2$; POPC: $a_\ell = 0.6212(3)\,\mathrm{nm}^2$). This results in a a quite sizable residual differential tension $\Sigma_{\mathrm{DLPC}} \approx -5.7\,\mathrm{mN/m}$ that puts the DLPC leaflet under compression. Nevertheless, the resulting asymmetric membrane has a bending rigidity that does not differ statistically significantly from the two pure cases and (more generally relevant) from their average. To test whether the sizable differential stress creates any artifacts, we also performed a simulation for a system in which this stress was relaxed by reducing the overabundance of DLPC lipids, resulting in a system with the differential stress $\Sigma_{\mathrm{DLPC},0} \approx -0.03(6)\,\mathrm{mN/m}$. We found its curvature rigidity to be $\kappa = 32.9(4)\,k_{\mathrm{B}}T$, which again agrees with the pure systems within statistics.

Having investigated stress-free compositional asymmetry, let us now explore the opposite case: a compositionally symmetric DLPC membrane in which the number of lipids differs between the two leaflets, thus rendering them stress-wise asymmetric. As a measure of number asymmetry we use the relative excess δn, defined as

$$\delta n := \frac{N_> - N_<}{N_> + N_<}\,, \tag{36}$$

where $N_>$ and $N_<$ are the number of lipids in the more or less populated leaflet, respectively. This measures the percentage by which each leaflet is over- or underfilled compared to the balanced average.

Our simulation results, summarized in Tab. 2 and illustrated in Fig. 3, show that for an asymmetry up to about $\delta n = 3.2\%$ the rigidity does not significantly differ from that of a stress-balanced bilayer, nor does it show any more curvature softening. (Observe that the differential stress at that point, about $\pm 8\,\mathrm{mN/m}$, is larger than the stress of our asymmetric area balanced $\frac{\mathrm{DLPC}}{\mathrm{POPC}}$ system.) However, for larger lipid number asymmetry there is a noticeable and sudden rise of κ, which increases by almost 50% at the largest asymmetry we tested, $\delta n = 6.7\%$. Near the transition, the fit to Eqn. (5), which is nonlinear in the curvature softening parameter δ, exhibits metastable minima (indicated as open symbols in Fig. 3). Together with the stable solutions, they support the scenario of a discontinuous stiffening transition, as illustrated by the drawn curve (an empirical guide to the eye, for which we have no descriptive theory). This transition is accompanied by a significant (and equally abrupt) increase in curvature softening, *i. e.* a jump to larger values of δ, leading to a length ℓ that is comparable to bilayer thickness, about 2.5 times larger than in the stress-balanced case. Remarkably, the sudden increase in curvature rigidity is *not* accompanied by jumps in the lipid order parameters $P_{2,>}$ and $P_{2,<}$ in the over- and under-filled leaflets, respectively. Instead, $P_{2,>}$ increases continuously (but slowly) up to about 5% asymmetry, while $P_{2,<}$ decreases by a comparable amount. Only at around 6% do these order parameters change more dramatically. The latter is driven by the gel transition, which is easily recognized by its strong signal in the specific heat, see Fig. 3a. However, by then the bilayer stiffening transition has long happened.

DISCUSSION

Compositional asymmetry alone does not stiffen membranes

We find that a compositionally asymmetric $\frac{\mathrm{DLPC}}{\mathrm{POPC}}$ membrane with sufficiently small differential stress is no stiffer than (the average of) its two symmetric counterparts, $\frac{\mathrm{DLPC}}{\mathrm{DLPC}}$ and $\frac{\mathrm{POPC}}{\mathrm{POPC}}$.

[3] Our MARTINI DLPC lipid is in terms of structure and force field identical to the MARTINI DMPC lipid studied in Ref. (65); even though here we use the updated martini_2.1 force field, while Ref. (65) used martini_2.0, the relevant bead-parameters are identical. Considering this, one may ask why the rigidity determined in the present paper is almost $6\,k_{\mathrm{B}}T$ (or 20%) larger. We attribute this to the new version of Gromacs, v5.1, and refer the reader to Reißer *et al.* (108) for a detailed discussion how this version differs in some important ways from its predecessors. To minimize artifacts due to time-saving measures (such as pushing for large integration time steps) we use conservative parameters whenever options arise. Nevertheless, the situation remains unfortunate, and so we profess ourselves agnostic about the "true" value of the rigidity of MARTINI lipids. However, this does not affect the *relative* changes we discuss in the present paper.

Table 2: Simulated systems and results for measured observables. Buckle length L, number of lipids in overfilled ($N_>$) and underfilled ($N_<$) leaflet, asymmetry, lipid order parameter in overfilled ($P_{2,<}$) and underfilled ($P_{2,>}$) leaflet, tension Σ_+ in the upper leaflet, bending rigidity κ, cross-over length ℓ in the curvature-softened energy density (4) and corresponding softening parameter $\delta = 2\pi\ell/L$. In all simulations the box width is $L_y = 8\,\mathrm{nm}$.

leaflets	L [nm]	$N_>/N_<$	δn [%]	c_p/k_B	$P_{2,>}$	$P_{2,<}$	Σ_+ [mN/m]	κ [$k_\mathrm{B}T$]	ℓ [nm]
DLPC/DLPC	41.39 ± 0.02	580/580	0	0.85 ± 0.02	0.699(1)	0.699(1)	0.07 ± 0.07	34.8 ± 1.1	2.0 ± 0.8
POPC/POPC	45.03 ± 0.02	580/580	0	n.d.	n.d.	n.d.	0.03 ± 0.07	34.4 ± 1.3	2.6 ± 0.9
DLPC/POPC	40.60 ± 0.03	568/522	4.22	n.d.	n.d.	n.d.	−5.68 ± 0.08	34.1 ± 0.9	1.7 ± 0.7
DLPC/POPC	40.02 ± 0.01	540/530	0.93	n.d.	n.d.	n.d.	−0.03 ± 0.06	32.9 ± 0.4	1.1 ± 0.4
DLPC/DLPC	39.50 ± 0.01	580/552	2.47	0.84 ± 0.01	0.715(1)	0.683(1)	−5.64 ± 0.08	33.6 ± 0.7	1.5 ± 0.7
DLPC/DLPC	40.17 ± 0.01	580/544	3.20	0.83 ± 0.01	0.718(1)	0.678(1)	−6.97 ± 0.07	34.5 ± 0.7	2.0 ± 0.5
DLPC/DLPC	39.91 ± 0.01	580/536	3.94	0.84 ± 0.01	0.722(1)	0.672(1)	−8.46 ± 0.08	44.1 ± 0.3	6.7 ± 0.2
DLPC/DLPC	39.50 ± 0.01	580/522	5.26	0.87 ± 0.01	0.729(1)	0.663(1)	−11.18 ± 0.09	47.0 ± 0.5	5.5 ± 0.1
DLPC/DLPC	37.38 ± 0.21	580/515	5.94	8.68 ± 4.63	0.765(6)	0.686(5)	−12.59 ± 0.06	47.0 ± 0.8	5.4 ± 0.1
DLPC/DLPC	33.93 ± 0.10	580/507	6.72	1.23 ± 0.31	0.853(1)	0.625(1)	−13.93 ± 0.09	50.2 ± 0.6	4.6 ± 0.1

Granted, a single example for the absence of stiffening does not rule it out for all conceivable cases. But it must be recalled that this is the expected outcome: as long as the two leaflets can freely slide, and their individual structure matches that of their symmetric bilayer counterparts, basic elasticity considerations demand that leaflet rigidities simply add. Hence, the burden of proof lies with any claim of stiffening, and our particular negative result merely establishes the expected baseline.

One might worry that our two lipids were elastically too similar to begin with, but the experimentally observed increase in bending modulus (factor ∼ 2.5, or about 150% stiffer) is much bigger than the disparity between the moduli of the two individual lipids (factor ∼ 1.3, or about 30% stiffer) (50, 51), and so it is unlikely that this is a major factor. In contrast, the two leaflets might influence each other more directly via their free energy of adhesion, which depends on their area per lipid. Since our two CG lipids differ by about 9% in that regard, this effect would be even slightly bigger than what the experimental difference between the lipids used in the stiffening studies (50, 51) (POPC and DOPC) would be—with DOPC having an area about 6% larger, when measured by the same technique (109).

Differential stress can stiffen membranes

What we instead find is that differential stress, if large enough, increases a bilayer's curvature modulus. Before addressing the origin of this effect, let us first rule out an incorrect attempt at a geometric explanation: could it be that the buckle of a differentially stressed membrane assumes some potentially asymmetric shape that strains the leaflets differently, thereby giving rise to a nonzero additional *stretching* contribution to the overall energy? The answer is no, because buckling does not globally strain the leaflets at all. To see why, let us calculate the membrane area $A_\pm$ of the upper and lower leaflet (taken for instance at their neutral surfaces $\pm z_\pm$), using the parallel surface theorem (10, 80):

$$A_\pm = \int \mathrm{d}A \left\{1 \pm z_\pm K + z_\pm^2 K_\mathrm{G}\right\} \tag{37a}$$

$$= A_\mathrm{mid} \pm z_\pm \int \mathrm{d}A\; K + z_\pm^2 \int \mathrm{d}A\; K_\mathrm{G}\,, \tag{37b}$$

where the integral is taken over the buckle's midplane, which has area A_mid, and where K_G is the Gaussian curvature. By the Gauss-Bonnet theorem (80), the integral over K_G is a topological invariant and hence coincides with its value for the unbuckled membrane, for which $K_\mathrm{G} = 0$; hence this term vanishes. And the integral over K can be rewritten to an excellent approximation by assuming that the buckle only significantly curves *along* the buckling direction, not perpendicularly to it.[4] In that case, we can describe the buckle by a single function $\psi(s)$, the angle against the horizontal as a function of arc length s. The curvature can then be expressed as $K = -\partial\psi(s)/\partial s$, and so we can simplify Eqn. (37b) to

$$A_\pm = A_\mathrm{mid} \mp z_\pm L_y \int_0^L \mathrm{d}s\; \frac{\partial\psi(s)}{\partial s} \tag{37c}$$

$$= A_\mathrm{mid} \mp z_\pm L_y \left[\psi(L) - \psi(0)\right] \tag{37d}$$

$$= A_\mathrm{mid}\,, \tag{37e}$$

where in the last step we exploited periodic boundary conditions: $\psi(0) = \psi(L)$. We hence see that in fact *any* leaflet reference surface (not just the neutral surface) keeps its area when buckled under periodic boundary conditions. Notice that this dos not even require the buckle's geometry to be the solution of some shape equation; *any* shape will do. The two additions in Eqn. (37b) both vanish identically—for (different) *topological* reasons. Evidently, this same argument also shows

[4] This is ensured in simulations by making the transverse direction L_y much smaller than the buckle's length L. Since the buckling threshold scales inversely with the square of the buckle's length, see Eqns. (3) or (5), the force at which the y-direction would buckle is bigger than the membrane's x-buckling threshold by a factor of $(L/L_y)^2$. It is hence easy to ensure that the membrane will be flat along the y-direction.

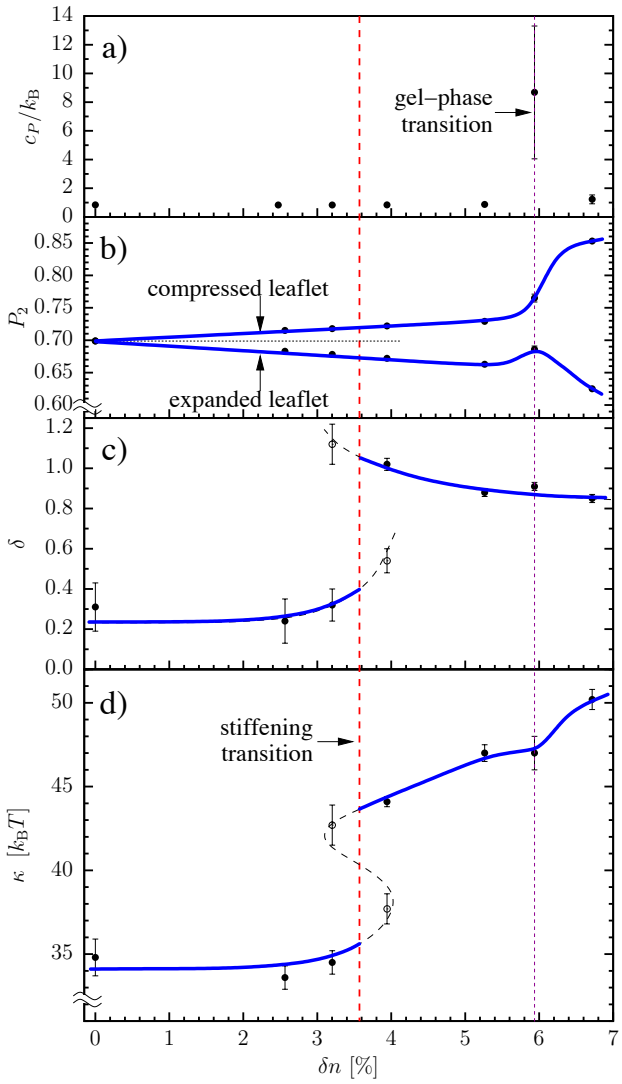

Figure 3: Several observables of differentially stressed MARTINI DLPC membranes as a function of asymmetry δn. Open symbols denote metastable states in the nonlinear fit; curves are guides to the eye. a) specific heat; b) orientational order parameter P_2; c) softening parameter δ; d) curvature modulus κ. The bold dashed vertical line suggests the approximate location of the stiffening transition, the dotted vertical line suggests the location at which the compressed leaflet transitions into the gel phase.

that the buckling protocol is insensitive to the spontaneous bilayer curvature: this only contributes a linear term in K to the energy density, which then vanishes under periodic boundary conditions.

Stressed leaflets differ elastically from unstressed ones

While our simulations clearly show that differential stress can stiffen a bilayer, the data by themselves do not yet offer an explanation for this observation. However, based on our collective findings we suggest that a stress-induced change in the elastic properties of the individual leaflets lies at the heart of the phenomenon. Recall that a major puzzle of the experimental results was the apparent "lack of additivity" (50): the rigidity of an asymmetric membrane is not the average of the corresponding two symmetric parent membranes. And yet, our own theoretical analysis always assumed additivity—see Eqns. (12) and (16a). This is no contradiction, though, because the differential stress generally present in asymmetric bilayers puts each of their leaflets into a thermodynamic state that differs from its counterpart in a stress-free symmetric bilayer. This of course also affects the leaflet rigidities, but it is unfortunately difficult to anticipate the magnitude of this change from measurements performed on symmetric membranes: the higher lipid density in the compressed leaflet cannot be recreated by laterally compressing a symmetric membrane, since it would relax the area strain via buckling; and while the lower lipid density in the expanded leaflet can in principle be produced by applying tension to a symmetric membrane, it is then difficult to measure its rigidity (for instance because tension would strongly suppress bending modes in a flicker spectroscopy experiment). This observation shows that additivity might well hold, but *we do not know what leaflet-rigidities we actually have to add*.

Nevertheless, it seems highly plausible that, *ceteris paribus*, membranes with a smaller area per lipid are stiffer than those with a larger one. But if this dependency were linear, then it would cancel in a differentially stressed membrane, in which to a very good approximation the area strains are simply opposite in sign. However, there are good reasons to believe that *for dense systems* the relation is not linear. Recall that for an ideal gas the isothermal bulk modulus $K_T = -V(\partial P/\partial V)_T$ is proportional to the density, but in the liquid phase of a van der Waals gas it grows much more strongly with density (in fact, it diverges at the maximal "close-packing" density). The same physics reappears in fluid lipid bilayers: polymer brush theory (88) shows that the lateral leaflet pressure Π is proportional to $1/a_\ell^3$, where a_ℓ is the specific lipid area; hence $K_A = -a_\ell(\partial\Pi/\partial a_\ell)_T = 3\Pi$ shows the same strong increase with compression.

In simulations, a clean way to reduce the area per lipid is to artificially increase the cohesive energy between lipids. This can be done quite easily in coarse-grained lipid models in which this cohesion is one of the few tuning parameters. For instance, doing exactly this in the coarse-grained Cooke model (110–112) shows that the curvature rigidity of fluid Cooke-membranes scales approximately *exponentially* with the lipid area density (to see this, combine the lower two panels of Fig. 7 in Ref. (111)). Hence, the stiffening of the

compressed leaflet overwhelms the softening of the expanded one, leading to an overall rigidity increase of differentially stressed membranes.

Stiffening is linked to the gel transition, but not identical with it

That a bilayer's curvature rigidity strongly increases with lipid density is particularly vivid in gel phase membranes, whose lipid density is typically about 30% higher than that of fluid phases, but whose rigidity is easily an order of magnitude larger (113–115). Curiously, gel phases also exhibit *much* stronger curvature softening than fluid phases ($\ell \approx 14$ nm for MARTINI DMPC (66)); in fact, the modified curvature energy density in Eqn. (4) that allows for softening, together with its stress-strain relation (5), was originally developed by Diggins *et al*. to describe gel phases (66). These authors also noticed that for coarse-grained models (such as MARTINI) $\kappa_{\mathrm{gel}}/\kappa_{\mathrm{fluid}}$ is not quite as large as seen in experiments—provided both phases are extrapolated to the transition temperature (116). This mirrors the finding in the present paper that the rigidity increase driven by differential stress (about 50%) is likewise not as large as the one that is experimentally observed (about 150%). Considering that coarse-grained models are typically designed to get the properties of fluid phases right, this discrepancy is not overly disturbing.

While the increase in membrane rigidity upon entering the gel phase is well established, our data nevertheless show quite clearly that the fluid-gel transition does *not* coincide with the stiffening transition: the latter happens much earlier, meaning, at smaller asymmetries δn. A transition of the compressed leaflet into the gel phase does ultimately happen—as evident visually, in the order parameter P_2, and the specific heat c_P—but only in our strongest asymmetric system, $\delta n = 6.7\%$.

We have no microscopic explanation for why these two transitions take place at different asymmetries or, presumably equivalently, different differential stresses.

We can visually identify small transient gel regions in the compressed leaflet even slightly *below* the transition, but not all the way down to the actual stiffening transition. These patches appear to prefer the vicinity of a buckle's inflection points, not its turning points. It is hence conceivable that their further growth is impeded by the curvature of the buckle, and that observations based on buckles might therefore exhibit some finite size effects. However, the two thermodynamic pieces of evidence we have presented for the gel-transition in the compressed leaflet—the specific heat c_P and the orientational order parameter P_2, both shown in Fig. 3—were determined for the uncompressed *flat* membrane at $\gamma = 0$, indicating that even in the absence of curvature gradients the overcrowded leaflet does not transition into the gel phase for $\delta n \lesssim 6\%$.

If transient gel or gel-like domains prefer the vicinity of inflection points, this would bias a buckle's shape to be flatter in these regions than expected for classical Euler elastica. Diggins *et al*. (66) captured precisely this feature in their curvature-softened buckling theory, where it shows up as an increase in ℓ or δ. This still leaves open the question whether in the present case it arises as a consequence of a "biphasic" membrane (as just described), or a "monophasic" membrane comprising a material with a fairly nonlinear elastic response (as Diggins *et al*. (66) concluded for pure gel phases). A further analysis of a buckle's position dependent orientational order parameter or area per lipid would likely shed more light onto this question. All the same, any flattening of the buckle near its inflection points (irrespective of the cause), and the associated non-Eulerian stress-strain response, prevents the fit from misreading the still soft turning points (or "hinges") as being representative of the entire membrane's rigidity.

Even more fundamentally, how a single-leaflet gel transitions takes place in such strongly differentially stressed bilayers is likely very subtle due to the competition between the two leaflets: upon increasing the asymmetry, the depleted one ever more strongly tries to compress the overfilled one, until the latter finally gives in; but when that happens, the concomitant reduction in area of the depleted leaflet also reduces its driving force for this very transition. In other words, it is not sufficient to picture the gel transition of the compressed leaflet as being driven by a fixed imposed stress. A refined analysis of this scenario will be left for a future study.

Creating compositionally asymmetric membranes can induce accidental differential stress

The experimental results of Elani *et al*. (50) suggest that compositionally asymmetric membranes are more rigid than their symmetric counterparts, while we instead argue that differential stress lies at the core of stiffening. But Elani *et al*. did not aim for differential stress; they expressly aimed for compositional asymmetry, and this is what the phase transfer protocol is supposed to produce. Moreover, Elani *et al*. were quite conscious of the possibility that the phase transfer protocol might generate undesired artifacts, and so they devised a control experiment in which they created *symmetric* membranes via the more elaborate layer-by-layer process—finding them to be elastically indistinguishable from symmetric membranes made by conventional electroformation. To explain why this negative outcome does not exclude the possibility of differential stress, we now discuss a scenario in which asymmetry is in fact a *prerequisite* for the phase transfer protocol to engender differential stress.

Consider, therefore, a compositionally asymmetric bilayer vesicle that is built by joining two individual leaflets, each initially present as a monolayer at an oil water interface (34–37, 42, 43). We will assume that the area per lipid in these monolayers is determined by some equilibrium condition (say, the equilibrium spreading pressure set by the chemical potential of lipids in the oil phase) and given by $a_{\mathrm{s}j}$ (where $j \in \{+,-\}$ labels the leaflets). The vesicle's initial area is then given by $A_{\mathrm{i}} = N_j a_{\mathrm{s}j}$ (for both j). The crucial point is that the

monolayer areas per lipid need not coincide with those in a stress-free leaflet of a lipid bilayer, a_{0j}, and therefore each leaflet harbors energy due to tangential stress, given by

$$E_{\text{stretch}} = \frac{1}{2}K_{A,\text{m}+}\frac{(A_\text{i} - N_+a_{0+})^2}{N_+a_{0+}} + \frac{1}{2}K_{A,\text{m}-}\frac{(A_\text{i} - N_-a_{0-})^2}{N_-a_{0-}} \,. \tag{38}$$

The vesicle can lower this energy, and hence eliminate the *net stress* Σ, by changing its initial area A_i to some final area A_f. The energy minimization condition $\Sigma = \partial E_{\text{stretch}}/\partial A_\text{f} = 0$ then leads to

$$\frac{A_\text{i}}{A_\text{f}} = \alpha_+\frac{a_{\text{s}+}}{a_{0+}} + \alpha_-\frac{a_{\text{s}-}}{a_{0-}} \,, \tag{39}$$

where we again defined $\alpha_j = K_{A,\text{m}j}/(K_{A,\text{m}+}+K_{A,\text{m}-})$. Eqn. (39) fixes the equilibrium areas per lipid, $a_j^* = A_\text{f}/N_j$, from which we can subsequently calculate the area strain $\gamma_\pm$ in each leaflet:

$$\gamma_\pm = \frac{a_\pm^*}{a_{0\pm}} - 1 = \alpha_\mp\,\frac{a_{\text{s}\pm}/a_{0\pm} - a_{\text{s}\mp}/a_{0\mp}}{\alpha_+\,a_{\text{s}+}/a_{0+} + \alpha_-a_{\text{s}-}/a_{0-}} \,. \tag{40}$$

Since $\Sigma_\pm = K_{A,\text{m}\pm}\gamma_\pm$, we readily verify that $\Sigma_+ + \Sigma_- = 0$. Moreover, with a fairly good approximation $\alpha_+ = \alpha_- = 1/2$, which permits the further simplification

$$\gamma_\pm = \pm\,\frac{r-1}{r+1} \qquad \text{with} \qquad r = \frac{a_{\text{s}+}/a_{0+}}{a_{\text{s}-}/a_{0-}} \,, \tag{41}$$

showing that at this level even the strains add to zero.

Notice now that the two ratios $a_{\text{s}j}/a_{0j}$ quantify the extent to which the area per lipid differs between a monolayer and a single stress-free leaflet in a bilayer. This ratio depends on the lipid composition of the leaflet (and the experimental conditions for the respective monolayers), and so the ratio r of these two ratios generally differs from 1 when asymmetric membranes are created in a layer-by-layer process. Eqn. (41) then explains how the two leaflets inherit a nonzero area strain and a *differential stress*, even after the *net stress* has relaxed. However, if we create a symmetric membrane by this layer-by-layer process, the two ratios $a_{\text{s}j}/a_{0j}$ will be identical, implying $r = 1$ and $\gamma_\pm = 0$. This shows that even though the phase transfer protocol starts out with two monolayers, neither of which need reproduce the correct area per lipid for a bilayer, the symmetric control experiment actually restores the stress balance. If stiffening really results from differential stress, symmetric vesicles produced in this way would not show stiffening—in agreement with the actual observation (50).

There is another observation which suggests that at least *some* differential stress ought to have been present in the vesicles of Elani *et al.*: recall from our earlier discussion that an asymmetric $\frac{\text{DOPC}}{\text{POPC}}$ membrane in the absence of differential stress should have a spontaneous curvature of $K_{0\text{b}} \approx -0.017\,\text{nm}^{-1}$. Since the giant unilamellar vesicles used in these experiments had radii of about $R_0 \sim 20\,\mu\text{m}$, this implies a huge reduced spontaneous curvature $|R_0K_{0\text{b}}| \sim 300 \gg 1$, which in turn indicates that these vesicles should have a very high tendency to tubulate. The fact that this was not observed suggests a differential stress which compensates the huge materials-based spontaneous curvature. As we have shown following Eqn. (20), the overall spontaneous curvature $K_0^\star$ gets reduced to zero when a tension of about $0.8\,\text{mN/m}$ is present.

Cholesterol need not cancel differential stress

Let us finally address the question whether a rapidly flip-flopping lipid species, such as in particular cholesterol, will distribute between the leaflets such as to eliminate any differential stress. This claim was recently made by Miettinen and Lipowsky (92), but we have argued in our theory section that the situation is likely more complex: since the elastic energy is only one of several contributions to cholesterol's chemical potential, it is not the only one that guides its distribution between leaflets. In particular, we have presented a simple model that shows how addition of cholesterol may not just fail to fully cancel a stress difference but actually *create* one—namely, if its free energy of partitioning differs sufficiently strongly between the leaflets.

To test the latter scenario in simulation, we have prepared a compositionally asymmetric bilayer of two lipid species with a significant difference in their ability to solvate cholesterol. One is DPPC, the other one DIPC (see Fig. 1). Since cholesterol prefers to partition into saturated phases (95), we expect it to have a preference for the DPPC side.

We started by simulating two symmetric mixed membranes that consisted of a 4:1 mixture of either DPPC or DIPC with cholesterol. Using the average area densities obtained this way, we then created an asymmetric membrane with a (4:1) DPPC+Chol mixture on one side (72 DPPC lipids and 18 cholesterols), and a (4:1) DIPC+Chol mixture on the other (56 DIPC lipids and 14 cholesterols). Evolving this system from this initial condition we observed a strong tendency for cholesterol to re-partition into the DPPC leaflet, with an approximately exponential kinetics characterized by a relaxation time of about 200 ns, as illustrated in Fig. 4. After less than 1 µs the DPPC leaflet holds about 25 cholesterol molecules, *i. e.* about 80% of the total cholesterol content. Checking the differential tension at this end point, we find that it has the value $\Sigma_\pm^{(\text{res})} = -3.71(88)\,\text{mN/m}$, leaving the DPPC+Chol leaflet under a noticeable compressive stress.

The key difference to the simulation presented by Miettinen and Lipowsky is our choice of lipid tails: we explicitly set up a situation in which cholesterol experiences a large differential free energy of partitioning Δg between the leaflets. This is not an unphysiological scenario, though. Consider for instance that the outer leaflet of a cell's plasma membrane contains all of the membrane's sphingomyelin, a strong cholestreol "recruiter". In fact Allender *et al.* (74) have estimated that this would drive almost 3/4 of the plasma membrane's cholesterol content into that leaflet, were it not for the elastic cost associated with cholesterol's change of a leaflet's spontaneous

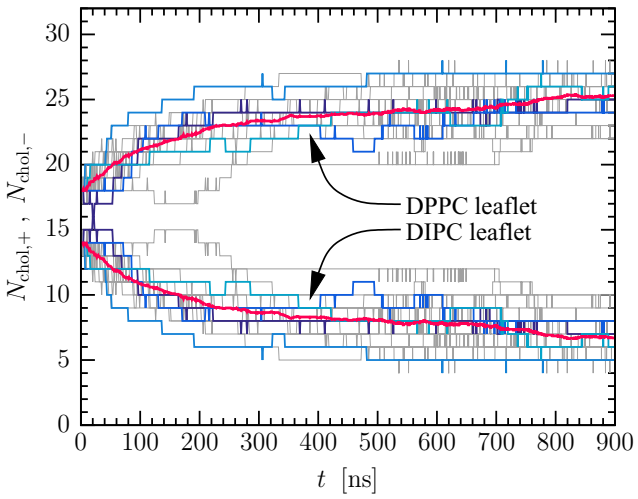

Figure 4: Number of cholesterol molecules $N_{\mathrm{chol},\pm}$ in the upper or lower leaflet of a $\frac{\text{DPPC+Chol}}{\text{DIPC+Chol}}$ bilayer as a function of time. The initial state contained 20% cholesterol per leaflet in an area-matched asymmetric system. Cholesterol flip-flop leads to a 25:7 redistribution with a relaxation time of about 200 ns. The graph illustrates 20 independent simulations, four of which are singled out in different shades of blue; the bold red curve is the average over all of them.

curvature, which turns out to counteract the driving force due to solvation. Under realistic situations the magnitude of this effect will depend on many other factors, and in a biological context it will of course be different for different membrane systems inside cells. But for now, our simple counter-example indicates that cholesterol will not automatically eliminate the differential stress of a membrane.

SUMMARY AND OUTLOOK

On time scales that are short compared to lipid flip-flop time, a membrane can exhibit two types of metastable asymmetry: one due to composition, the other one due to lateral stress. Hence, a characterization of bilayer asymmetry that merely addresses the compositional aspect is incomplete. However, these two asymmetries are not independent, and their interplay can lead to sometimes unexpected phenomena. An example is the residual tension in an area-balanced asymmetric membrane, for which our proposed theoretical framework suggests a simple and predictive explanation.

We have shown that asymmetric membranes can be significantly stiffer than what would be expected from their cognate symmetric partners. This was indeed found in recent experiments, but we argue that the cause of this effect is differential stress, not the composition asymmetry by itself. The likely mechanism involves the creation of a more highly ordered compressed leaflet, which we expect to be much stiffer and dominate the bilayer's energetic response to bending. This hypothesis is unfortunately difficult to test directly, especially in experiment, because such compressed phases cannot be recreated in symmetric systems, and we are not aware of means to probe a single leaflet's curvature elasticity directly.

Moreover, the stiffening transition appears to be linked to the gel transition, but it does not coincide with it. Since we have only investigated the case of DLPC at 300 K, we cannot make a general statement how the stiffening transition would pan out if the gel transition of the leaflet that ends up being compressed were closer or farther away from the zero tension state point. For instance, had we simulated the system at a lower temperature, we would expect—by Le Chatelier's principle—that it takes a smaller asymmetry to drive the compressed DLPC leaflet into the gel phase, thus decreasing the gap between the two transitions. Conversely, had we used a highly disordered lipid, such as DIPC, even a 6% asymmetry might not yet trigger the fluid-gel transition, thus widening the gap. In neither of these scenarios it is obvious how the stiffening transition happens, or whether it would even arise. Unveiling the interplay between these transitions should be a rewarding subject for future studies.

A stress imbalance between bilayer leaflets, and its impact on any number of membrane properties, is a matter of practical concern, since recently proposed methods for creating compositionally asymmetric membranes might inadvertently also render them differentially stressed. We have explicitly shown how this might happen in the phase transfer protocol, but it is not difficult to imagine causes for imbalance that arise in the lipid exchange protocol. In fact, in many cases of practical relevance a bilayer's spontaneous materials curvature $K_{0\mathrm{b}}$ is so large that macroscopic membrane systems (such as giant unilamellar vesicles, especially deflated ones) should be unstable against tubulation without a counterbalancing differential stress.

We have finally shown that incorporating lipid species that can rapidly transition between leaflets, such as cholesterol, renders the situation even more complex. One possibility is that their redistribution expunges differential stress, as recently observed by Miettinen and Lipowsky, but this is not the generic outcome. The chemical potential of these molecules may contain contributions that expressly favor their uneven distribution between leaflets, and so adding them to a stress-balanced membrane might actually create differential stress. In the case of cholesterol this can easily happen when the two leaflets differ in their tail order, as is for instance the case in the plasma membrane.

Evidently, all this matters beyond the case of simple biophysical model systems, since virtually all biomembranes are known to be compositionally asymmetric. Our observations hence pose a number of pertinent questions: are such membranes also differentially stressed? Their cholesterol content might not protect them from such a state. If they are stressed, is their curvature rigidity higher than what we would otherwise deduce from their components? Maybe by a lot? Since we know that nature deliberately controls and maintains the

composition aspect of biomembrane asymmetry, does it also control differential stress? If so, would it do so actively (say, by expressly "overfilling" a leaflet), or passively by exploiting that stress imbalance can be induced by a mismatch between shape and spontaneous curvature?

These questions strike us as highly relevant for understanding the morphology and energetics of cellular membrane systems, and so it is all the more distressing that no adequate simulational or experimental techniques appear to exist that can address them at this point. Simulations can of course study any type of asymmetric membranes and hence increase our understanding of these systems; but this cannot answer the question what state of asymmetry is actually realized in nature's biomembranes. And experiments face the difficulty that we do not know how to readily measure membrane stress *in vivo*, let alone on a single leaflet basis. Recently proposed fluorescent reporters of membrane tension (117) might be a way into the right direction, but we would then need to know better what these molecules actually report (most likely: local order), and how to confine them to a single leaflet. Alternatively, the force required to pull a cylindrical ("wormlike") micelle out of a single leaflet depends on its tension (118), but it will then be even more important than in conventional tether pulling experiments to disentangle the kinetic contribution (due to inter-leaflet friction) from the stress-strain relation.

The recently developed experimental protocols for manufacturing asymmetric model membranes have rightfully sparked a renaissance of the subject, and we hence expect that these challenges will be tackled. Until then, simulation and theory can do two things: first, help to provide a deeper understanding of the issues that need addressing; and second, suggest observables that are informative about the situation and could maybe even serve as proxies for differential stress. Our goal in this paper was to make steps into this direction.

AUTHOR CONTRIBUTIONS

MD suggested the subject and acquired funding for it. AH performed all molecular dynamics simulations and data analysis. MD and AH discussed the findings and decided on the research direction. MD developed the theory and wrote the paper.

ACKNOWLEDGMENTS

The authors would like to thank Juan Vanegas for useful feedback on GROMACS-LS, and Helgi Ingólfsson for providing a refined MARTINI cholesterol topology that eliminated the need for virtual sites and could hence be processed by (the current version of) GROMACS-LS. MD also gratefully acknowledges support by the National Science Foundation via grant CHE 1764257.

GLOSSARY

For the convenience of the reader, this glossary gives a list of the most common mathematical symbols and notations we use. The list is not complete but focuses on those cases where confusions are most likely to arise.

Symbol	Description
$\pm$	subscript denoting upper (+) or lower (−) leaflet
$\alpha_\pm$	fraction of membrane expansion modulus due to ±-leaflet, $= K_{A,\mathrm{m}\pm}/K_A$
α_{sc}	stress-curvature parameter, Eqn. (21)
$\mathcal{A}_\pm$	equilibrium area of a mixed (flat) leaflet, Eqn. (27)
d	total bilayer thickness
d_{h}	thickness of a bilayer's hydrophobic region
$g_\pm$	cholesterol partitioning free energy into ± leaflet, Eqn. (27)
Δg	cholesterol partitioning difference, $= g_+ - g_-$
γ	buckling strain, Eqn. (1)
K	curvature of bilayer, measured at midplane
$K_{A,\mathrm{m}\pm}$	monolayer area expansion modulus, Eqn. (16a)
K_A	bilayer area expansion modulus, $= K_{A,+} + K_{A,-}$
$K_{0\mathrm{b}}$	a bilayer's spontaneous materials curvature, created due to lipid curvature, Eqn. (13)
$K_{0\mathrm{s}}$	bilayer curvature at which differential stress vanishes, Eqn. (15)
$K_0^\star$	bilayer curvature at which overall bending and stretching energy is minimized, Eqn. (18)
$K_{\mathrm{m}\pm}$	spontaneous leaflet curvature due to lipids, Eqn. (12)
κ	bilayer curvature modulus, Eqn. (14)
κ_{nl}	nonlocal bilayer curvature modulus, Eqn. (16d)
$\kappa_{\mathrm{m}\pm}$	monolayer curvature modulus, Eqn. (12)
ℓ	curvature crossover length, Eqn. (4)
Σ	net bilayer tension, $= \Sigma_+ + \Sigma_-$
$\Sigma_\pm$	individual leaflet tension
$\Sigma_\pm^{(\mathrm{res})}$	residual differential stress in an area balanced membrane, Eqn. (24)
$z_\pm$	distance of upper (+) or lower (−) neutral surface from bilayer midplane
z_0	value of $z_\pm$ if we assume $z_+ \approx z_-$

REFERENCES

1. Bassereau, P., R. Jin, T. Baumgart, M. Deserno, R. Dimova, V. A. Frolov, P. V. Bashkirov, H. Grubmüller, R. Jahn, H. J. Risselada, L. Johannes, M. M. Kozlov, R. Lipowsky, T. J. Pucadyil, W. F. Zeno, J. C. Stachowiak, D. Stamou, A. Breuer, L. Lauritsen, C. Simon, C. Sykes, G. A. Voth, and T. R. Weikl, 2018. The 2018 biomembrane curvature and remodeling roadmap. *J. Phys. D: Appl. Phys.* 51:343001.

2. Karp, G., 2013. Cell and molecular biology: concepts and experiments. John Wiley & Sons, 7 edition.

3. Alberts, B., A. Johnson, J. Lewis, D. Morgan, M. Raff, K. Roberts, and P. Walter, 2015. Molecular Biology of the Cell. Garland Science, New York, 6 edition.

4. Lodish, H., A. Berk, C. A. Kaiser, M. Krieger, A. Bretscher, H. Ploegh, A. Amon, and K. C. Martin, 2016. Molecular Cell Biology. W. H. Freeman, New York, 8 edition.

5. Helfrich, W., 1973. Elastic properties of lipid bilayers: theory and possible experiments. *Z. Naturforsch. C* 28:693–703.

6. Lipowsky, R., 1991. The conformation of membranes. *Nature* 349:475.

7. Seifert, U., 1997. Configurations of fluid membranes and vesicles. *Adv. Phys.* 46:13–137.

8. Zhong-Can, O.-Y., L. Jixing, and X. Yuzhang, 1999. Geometric methods in the elastic theory of membranes in liquid crystal phases, volume 2. World Scientific, Singapore.

9. Capovilla, R., and J. Guven, 2002. Stresses in lipid membranes. *J. Phys. A: Math. Gen.* 35:6233.

10. Deserno, M., 2015. Fluid lipid membranes: From differential geometry to curvature stresses. *Chem. Phys. Lipids* 185:11–45.

11. Singer, S. J., and G. L. Nicolson, 1972. The fluid mosaic model of the structure of cell membranes. *Science* 175:720–731.

12. Phillips, R., T. Ursell, P. Wiggins, and P. Sens, 2009. Emerging roles for lipids in shaping membrane-protein function. *Nature* 459:379.

13. Iversen, L., S. Mathiasen, J. B. Larsen, and D. Stamou, 2015. Membrane curvature bends the laws of physics and chemistry. *Nat. Chem. Biol.* 11:822.

14. Simons, K., and E. Ikonen, 1997. Functional rafts in cell membranes. *Nature* 387:569.

15. Brown, D. A., and E. London, 1998. Structure and origin of ordered lipid domains in biological membranes. *J. mem. Biol.* 164:103–114.

16. Brown, D. A., and E. London, 1998. Functions of lipid rafts in biological membranes. *Ann. Rev. Cell Develop. Biol.* 14:111–136.

17. Lingwood, D., and K. Simons, 2010. Lipid rafts as a membrane-organizing principle. *Science* 327:46–50.

18. Munro, S., 2003. Lipid rafts: elusive or illusive? *Cell* 115:377–388.

19. Almeida, P. F., A. Pokorny, and A. Hinderliter, 2005. Thermodynamics of membrane domains. *Biochim. Biophys. Acta, Biomembr.* 1720:1–13.

20. Niemelä, P. S., S. Ollila, M. T. Hyvönen, M. Karttunen, and I. Vattulainen, 2007. Assessing the nature of lipid raft membranes. *PLoS Comp.Biol.* 3:e34.

21. Fan, J., M. Sammalkorpi, and M. Haataja, 2010. Formation and regulation of lipid microdomains in cell membranes: theory, modeling, and speculation. *FEBS Lett.* 584:1678–1684.

22. Levental, I., and S. L. Veatch, 2016. The continuing mystery of lipid rafts. *J. Mol. Biol.* 428:4749–4764.

23. Sezgin, E., I. Levental, S. Mayor, and C. Eggeling, 2017. The mystery of membrane organization: composition, regulation and roles of lipid rafts. *Nat. Rev. Mol. Cell Biol.* 18:361.

24. Bretscher, M. S., 1972. Asymmetrical lipid bilayer structure for biological membranes. *Nature New Biol.* 236:11.

25. Op den Kamp, J. A. F., 1979. Lipid asymmetry in membranes. *Annu. Rev. Biochem.* 48:47–71.

26. Daleke, D. L., 2003. Regulation of transbilayer plasma membrane phospholipid asymmetry. *J. Lipid Res.* 44:233–242.

27. Van Meer, G., D. R. Voelker, and G. W. Feigenson, 2008. Membrane lipids: where they are and how they behave. *Nature Rev. Mol. Cell Biol.* 9:112.

28. Ingólfsson, H. I., M. N. Melo, F. J. Van Eerden, C. Arnarez, C. A. Lopez, T. A. Wassenaar, X. Periole, A. H. De Vries, D. P. Tieleman, and S. J. Marrink, 2014. Lipid organization of the plasma membrane. *J. Am. Chem. Soc.* 136:14554–14559.

29. Lipowsky, R., and H.-G. Döbereiner, 1998. Vesicles in contact with nanoparticles and colloids. *EPL (Europhys. Lett.* 43:219.

30. Döbereiner, H.-G., O. Selchow, and R. Lipowsky, 1999. Spontaneous curvature of fluid vesicles induced by trans-bilayer sugar asymmetry. *Eur. Biophys. J.* 28:174–178.

31. Różycki, B., and R. Lipowsky, 2015. Spontaneous curvature of bilayer membranes from molecular simulations: Asymmetric lipid densities and asymmetric adsorption. *J. Chem. Phys.* 142:02B601_1.

32. Różycki, B., and R. Lipowsky, 2016. Membrane curvature generated by asymmetric depletion layers of ions, small molecules, and nanoparticles. *J. Chem. Phys.* 145:074117.

33. Karimi, M., J. Steinkühler, D. Roy, R. Dasgupta, R. Lipowsky, and R. Dimova, 2018. Asymmetric ionic conditions generate large membrane curvatures. *Nano Lett.* 18:7816–7821.

34. Pautot, S., B. J. Frisken, and D. A. Weitz, 2003. Engineering asymmetric vesicles. *Proc. Nat. Acad. Sci. (USA)* 100:10718–10721.

35. Hamada, T., Y. Miura, Y. Komatsu, Y. Kishimoto, M. Vestergaard, and M. Takagi, 2008. Construction of asymmetric cell-sized lipid vesicles from lipid-coated water-in-oil microdroplets. *J. Phys. Chem. B* 112:14678–14681.

36. Hu, P. C., S. Li, and N. Malmstadt, 2011. Microfluidic fabrication of asymmetric giant lipid vesicles. *ACS Appl. Mater. Inter.* 3:1434–1440.

37. Matosevic, S., and B. M. Paegel, 2013. Layer-by-layer cell membrane assembly. *Nature Chem.* 5:958.

38. Cheng, H.-T., Megha, and E. London, 2009. Preparation and properties of asymmetric vesicles that mimic cell membranes effect upon lipid raft formation and transmembrane helix orientation. *J. Biol. Chem.* 284:6079–6092.

39. Cheng, H.-T., and E. London, 2011. Preparation and properties of asymmetric large unilamellar vesicles: interleaflet coupling in asymmetric vesicles is dependent on temperature but not curvature. *Biophys. J.* 100:2671–2678.

40. Chiantia, S., P. Schwille, A. S. Klymchenko, and E. London, 2011. Asymmetric GUVs prepared by MβCD-mediated lipid exchange: an FCS study. *Biophys. J.* 100:L1–L3.

41. Doktorova, M., F. A. Heberle, B. Eicher, R. F. Standaert, J. Katsaras, E. London, G. Pabst, and D. Marquardt, 2018. Preparation of asymmetric phospholipid vesicles for use as cell membrane models. *Nature protocols* 13:2086.

42. Elani, Y., A. Gee, R. V. Law, and O. Ces, 2013. Engineering multi-compartment vesicle networks. *Chem. Sci.* 4:3332–3338.

43. Elani, Y., R. V. Law, and O. Ces, 2014. Vesicle-based artificial cells as chemical microreactors with spatially segregated reaction pathways. *Nat. Comm.* 5:5305.

44. Noireaux, V., and A. Libchaber, 2004. A vesicle bioreactor as a step toward an artificial cell assembly. *Proc. Nat. Acad. Sci. (USA)* 101:17669–17674.

45. Noireaux, V., Y. T. Maeda, and A. Libchaber, 2011. Development of an artificial cell, from self-organization to computation and self-reproduction. *Proc. Nat. Acad. Sci. (USA)* 108:3473–3480.

46. Stano, P., G. Rampioni, P. Carrara, L. Damiano, L. Leoni, and P. L. Luisi, 2012. Semi-synthetic minimal cells as a tool for biochemical ICT. *Biosys.* 109:24–34.

47. Carrara, P., P. Stano, and P. L. Luisi, 2012. Giant vesicles "colonies": a model for primitive cell communities. *ChemBioChem* 13:1497–1502.

48. Zhang, Z., Z. Li, W. Yu, K. Li, Z. Xie, and Z. Shi, 2013. Propulsion of liposomes using bacterial motors. *Nanotech.* 24:185103.

49. Hadorn, M., E. Boenzli, K. T. Sørensen, D. De Lucrezia, M. M. Hanczyc, and T. Yomo, 2013. Defined DNA-mediated assemblies of gene-expressing giant unilamellar vesicles. *Langmuir* 29:15309–15319.

50. Elani, Y., S. Purushothaman, P. J. Booth, J. M. Seddon, N. J. Brooks, R. V. Law, and O. Ces, 2015. Measurements of the effect of membrane asymmetry on the mechanical properties of lipid bilayers. *Chem. Comm.* 51:6976–6979.

51. Karamdad, K., R. Law, J. Seddon, N. Brooks, and O. Ces, 2016. Studying the effects of asymmetry on the bending rigidity of lipid membranes formed by microfluidics. *Chem. Comm.* 52:5277–5280.

52. Marrink, S. J., H. J. Risselada, S. Yefimov, D. P. Tieleman, and A. H. De Vries, 2007. The MARTINI force field: coarse grained model for biomolecular simulations. *J. Phys. Chem. B* 111:7812–7824.

53. Marrink, S. J., and D. P. Tieleman, 2013. Perspective on the MARTINI model. *Chem. Soc. Rev.* 42:6801–6822.

54. Steinkühler, J., P. De Tillieux, R. L. Knorr, R. Lipowsky, and R. Dimova, 2018. Charged giant unilamellar vesicles prepared by electroformation exhibit nanotubes and transbilayer lipid asymmetry. *Sci. Rep.* 8:11838.

55. Duncan, S. L., I. S. Dalal, and R. G. Larson, 2011. Molecular dynamics simulation of phase transitions in model lung surfactant monolayers. *Biochim. Biophys. Acta, Biomembr.* 1808:2450–2465.

56. Waheed, Q., R. Tjörnhammar, and O. Edholm, 2012. Phase transitions in coarse-grained lipid bilayers containing cholesterol by molecular dynamics simulations. *Biophys. J.* 103:2125–2133.

57. Melo, M. N., H. I. Ingólfsson, and S. J. Marrink, 2015. Parameters for Martini sterols and hopanoids based on a virtual-site description. *J. Chem. Phys.* 143:243152.

58. Ollila, O. H. S., H. J. Risselada, M. Louhivuori, E. Lindahl, I. Vattulainen, and S. J. Marrink, 2009. 3D pressure field in lipid membranes and membrane-protein complexes. *Phys. Rev. Lett.* 102:078101.

59. Vanegas, J. M., A. Torres-Sánchez, and M. Arroyo, 2014. Importance of force decomposition for local stress calculations in biomembrane molecular simulations. *J. Chem. Theory Comput.* 10:691–702.

60. Ingólfsson, H. I. (in preparation).

61. Abraham, M. J., T. Murtola, R. Schulz, S. Páll, J. C. Smith, B. Hess, and E. Lindahl, 2015. GROMACS: High performance molecular simulations through multi-level parallelism from laptops to supercomputers. *SoftwareX* 1:19–25.

62. Abraham, M., D. van der Spoel, E. Lindahl, B. Hess, and the GROMACS development team, 2016. GROMACS User Manual version 2016-rc1. www.gromacs.org.

63. Berendsen, H. J. C., J. P. M. v. Postma, W. F. van Gunsteren, A. R. H. J. DiNola, and J. R. Haak, 1984. Molecular dynamics with coupling to an external bath. *J. Chem. Phys* 81:3684–3690.

64. Noguchi, H., 2011. Anisotropic surface tension of buckled fluid membranes. *Phys. Rev. E* 83:061919.

65. Hu, M., P. Diggins IV, and M. Deserno, 2013. Determining the bending modulus of a lipid membrane by simulating buckling. *J. Chem. Phys.* 138:214110.

66. Diggins IV, P., Z. A. McDargh, and M. Deserno, 2015. Curvature softening and negative compressibility of gel-phase lipid membranes. *J. Am. Chem. Soc.* 137:12752–12755.

67. Rowlinson, J. S., and B. Widom, 2002. Molecular Theory of Capillarity. Dover, Mineola, NY.

68. Hu, M., D. H. de Jong, S. J. Marrink, and M. Deserno, 2013. Gaussian curvature elasticity determined from global shape transformations and local stress distributions: a comparative study using the MARTINI model. *Faraday Discuss.* 161:365–382.

69. Helfrich, W., 1981. Amphiphilic mesophases made of defects. *In* R. Balian, M. Kléman, and J. P. Poirier, editors, Physics of Defects, North Holland, Amsterdam.

70. Szleifer, I., D. Kramer, A. Ben-Shaul, W. M. Gelbart, and S. A. Safran, 1990. Molecular theory of curvature elasticity in surfactant films. *J. Chem. Phys.* 92:6800–6817.

71. Hamm, M., and M. M. Kozlov, 2000. Elastic energy of tilt and bending of fluid membranes. *Eur. Phys. J. E* 3:323–335.

72. Dasgupta, R., M. S. Miettinen, N. Fricke, R. Lipowsky, and R. Dimova, 2018. The glycolipid GM1 reshapes asymmetric biomembranes and giant vesicles by curvature generation. *Proc. Nat. Acad. Sci. (USA)* 115:5756–5761.

73. Sreekumari, A., and R. Lipowsky, 2018. Lipids with bulky head groups generate large membrane curvatures by small compositional asymmetries. *J. Chem. Phys.* 149:084901.

74. Allender, D. W., A. J. Sodt, and M. Schick, 2019. Cholesterol-dependent bending energy is important in cholesterol distribution of the plasma membrane. *Biophys. J.* 116:2356–2366.

75. Venable, R. M., F. L. Brown, and R. W. Pastor, 2015. Mechanical properties of lipid bilayers from molecular dynamics simulation. *Chem. Phys. Lipids* 192:60–74.

76. Sperotto, M. M., and A. Ferrarini, 2017. Spontaneous Lipid Flip-Flop in Membranes: A Still Unsettled Picture from Experiments and Simulations. *In* R. M. Epand, and J.-M. Ruysschaert, editors, The Biophysics of Cell Membranes: Biological Consequences, Springer Singapore, Singapore, 29–60.

77. Traïkia, M., D. E. Warschawski, O. Lambert, J.-L. Rigaud, and P. F. Devaux, 2002. Asymmetrical membranes and surface tension. *Biophys. J.* 83:1443–1454.

78. Esteban-Martín, S., H. J. Risselada, J. Salgado, and S. J. Marrink, 2009. Stability of asymmetric lipid bilayers assessed by molecular dynamics simulations. *J. Am. Chem. Soc.* 131:15194–15202.

79. Park, S., A. H. Beaven, J. B. Klauda, and W. Im, 2015. How tolerant are membrane simulations with mismatch in area per lipid between leaflets? *J. Chem. Theory Comput.* 11:3466–3477.

80. Do Carmo, M. P., 2016. Differential Geometry of Curves and Surfaces: Revised and Updated Second Edition. Dover.

81. Evans, E. A., 1974. Bending resistance and chemically induced moments in membrane bilayers. *Biophys. J.* 14:923–931.

82. Evans, E. A., 1980. Minimum energy analysis of membrane deformation applied to pipet aspiration and surface adhesion of red blood cells. *Biophys. J.* 30:265–284.

83. Svetina, S., M. Brumen, and B. Zeks, 1985. Lipid bilayer elasticity and the bilayer couple interpretation of red-cell shape transformations and lysis. *Stud. Biophys.* 110:177–184.

84. Seifert, U., L. Miao, H.-G. Döbereiner, and M. Wortis, 1992. Budding transition for bilayer fluid vesicles with area-difference elasticity. *In* R. Lipowsky, D. Richter, and K. Kremer, editors, The structure and conformation of amphiphilic membranes, Springer, 93–96.

85. Heinrich, V., S. Svetina, and B. Žekš, 1993. Nonaxisymmetric vesicle shapes in a generalized bilayer-couple model and the transition between oblate and prolate axisymmetric shapes. *Phys. Rev. E* 48:3112.

86. Miao, L., U. Seifert, M. Wortis, and H.-G. Döbereiner, 1994. Budding transitions of fluid-bilayer vesicles: the effect of area-difference elasticity. *Phys. Rev. E* 49:5389.

87. Kozlov, M. M., and M. Winterhalter, 1991. Elastic moduli for strongly curved monoplayers. Position of the neutral surface. *J. Phys. II (France)* 1:1077–1084.

88. Rawicz, W., K. Olbrich, T. McIntosh, D. Needham, and E. Evans, 2000. Effect of chain length and unsaturation on elasticity of lipid bilayers. *Biophys. J.* 79:328–339.

89. Rand, R. P., N. L. Fuller, S. M. Gruner, and V. A. Parsegian, 1990. Membrane curvature, lipid segregation, and structural transitions for phospholipids under dual-solvent stress. *Biochemistry* 29:76–87.

90. Leikin, S., M. M. Kozlov, N. L. Fuller, and R. P. Rand, 1996. Measured effects of diacylglycerol on structural and elastic properties of phospholipid membranes. *Biophys. J.* 71:2623–2632.

91. Doktorova, M., and H. Weinstein, 2018. Accurate in silico modeling of asymmetric bilayers based on biophysical principles. *Biophys. J.* 115:1638–1643.

92. Miettinen, M. S., and R. Lipowsky, 2019. Bilayer membranes with frequent flip-flops have tensionless leaflets. *Nano letters* 19:5011–5016.

93. Campelo, F., C. Arnarez, S. J. Marrink, and M. M. Kozlov, 2014. Helfrich model of membrane bending: from Gibbs theory of liquid interfaces to membranes as thick anisotropic elastic layers. *Adv. Colloid Interface Sci.* 208:25–33.

94. Bennett, W. F. D., J. L. MacCallum, M. J. Hinner, S. J. Marrink, and D. P. Tieleman, 2009. Molecular view of cholesterol flip-flop and chemical potential in different membrane environments. *J. Am. Chem. Soc.* 131:12714–12720.

95. Zhang, Z., L. Lu, and M. L. Berkowitz, 2008. Energetics of cholesterol transfer between lipid bilayers. *J. Phys. Chem. B* 112:3807–3811.

96. Edholm, O., and J. F. Nagle, 2005. Areas of molecules in membranes consisting of mixtures. *Biophys. J.* 89:1827–1832.

97. Sodt, A., R. Venable, E. Lyman, and R. Pastor, 2016. Nonadditive compositional curvature energetics of lipid bilayers. *Phys. Rev. Lett.* 117:138104.

98. McIntosh, T. J., 1978. The effect of cholesterol on the structure of phosphatidylcholine bilayers. *Biochim. Biophys. Acta, Biomembr.* 513:43–58.

99. Hung, W.-C., M.-T. Lee, F.-Y. Chen, and H. W. Huang, 2007. The condensing effect of cholesterol in lipid bilayers. *Biophys. J.* 92:3960–3967.

100. Kučerka, N., J. D. Perlmutter, J. Pan, S. Tristram-Nagle, J. Katsaras, and J. N. Sachs, 2008. The effect of cholesterol on short-and long-chain monounsaturated lipid bilayers as determined by molecular dynamics simulations and X-ray scattering. *Biophys. J.* 95:2792–2805.

101. Leeb, F., and L. Maibaum, 2018. Spatially Resolving the Condensing Effect of Cholesterol in Lipid Bilayers. *Biophys. J.* 115:2179–2188.

102. Chen, Z., and R. P. Rand, 1997. The influence of cholesterol on phospholipid membrane curvature and bending elasticity. *Biophys. J.* 73:267–276.

103. Song, J., and R. E. Waugh, 1993. Bending rigidity of SOPC membranes containing cholesterol. *Biophys. J.* 64:1967–1970.

104. Henriksen, J., A. C. Rowat, and J. H. Ipsen, 2004. Vesicle fluctuation analysis of the effects of sterols on membrane bending rigidity. *Eur. Biophys. J.* 33:732–741.

105. Pan, J., T. T. Mills, S. Tristram-Nagle, and J. F. Nagle, 2008. Cholesterol perturbs lipid bilayers nonuniversally. *Phys. Rev. Lett* 100:198103.

106. Pan, J., S. Tristram-Nagle, and J. F. Nagle, 2009. Effect of cholesterol on structural and mechanical properties of membranes depends on lipid chain saturation. *Phys. Rev. E* 80:021931.

107. Gracià, R. S., N. Bezlyepkina, R. L. Knorr, R. Lipowsky, and R. Dimova, 2010. Effect of cholesterol on the rigidity of saturated and unsaturated membranes: fluctuation and electrodeformation analysis of giant vesicles. *Soft Matter* 6:1472–1482.

108. Reißer, S., D. Poger, M. Stroet, and A. E. Mark, 2017. Real cost of speed: the effect of a time-saving multiple-time-stepping algorithm on the accuracy of molecular dynamics simulations. *J. Chem. Theory Comput.* 13:2367–2372.

109. Kučerka, N., S. Tristram-Nagle, and J. F. Nagle, 2006. Structure of fully hydrated fluid phase lipid bilayers with monounsaturated chains. *J. Membr. Biol.* 208:193–202.

110. Cooke, I. R., K. Kremer, and M. Deserno, 2005. Tunable generic model for fluid bilayer membranes. *Phys. TRevical Review E* 72:011506.

111. Cooke, I. R., and M. Deserno, 2005. Solvent-free model for self-assembling fluid bilayer membranes: stabilization of the fluid phase based on broad attractive tail potentials. *J. Chem. Phys.* 123:224710.

112. Deserno, M., 2009. Mesoscopic membrane physics: concepts, simulations, and selected applications. *Macromol. Rapid Comm.* 30:752–771.

113. Lee, C.-H., W.-C. Lin, and J. Wang, 2001. All-optical measurements of the bending rigidity of lipid-vesicle membranes across structural phase transitions. *Phys. Rev. E* 64:020901.

114. Dimova, R., B. Pouligny, and C. Dietrich, 2000. Pretransitional effects in dimyristoylphosphatidylcholine vesicle membranes: optical dynamometry study. *Biophys. J.* 79:340–356.

115. Steltenkamp, S., M. M. Müller, M. Deserno, C. Hennesthal, C. Steinem, and A. Janshoff, 2006. Mechanical properties of pore-spanning lipid bilayers probed by atomic force microscopy. *Biophys. J.* 91:217–226.

116. Diggins IV, P., 2016. Investigation of Elastic Properties of Lipids and Proteins using Computer Simulations. Ph.D. thesis, Carnegie Mellon University, (unpublished).

117. Colom, A., E. Derivery, S. Soleimanpour, C. Tomba, M. Dal Molin, N. Sakai, M. González-Gaitán, S. Matile, and A. Roux, 2018. A fluorescent membrane tension probe. *Nature Chem.* 10:1118.

118. Zhang, G., and M. Müller, 2017. Rupturing the hemi-fission intermediate in membrane fission under tension: Reaction coordinates, kinetic pathways, and free-energy barriers. *J. Chem. Phys.* 147:064906.